# Numerical analyses of crack path instabilities in quenched plates

Maurizio M. Chiaramonte<sup>a</sup>, Benjamin E. Grossman-Ponemon<sup>b</sup>, Leon M. Keer<sup>c</sup>, Adrian J. Lew<sup>b,\*</sup>

<sup>a</sup>Department of Civil and Environmental Engineering, Princeton University, Princeton, NJ 08544
 <sup>b</sup>Department of Mechanical Engineering, Stanford University, Stanford CA 94305, USA
 <sup>c</sup>Department of Mechanical Engineering, Northwestern University, Evanston IL 60208, USA

#### Abstract

Crack path instabilities are observed in rapidly quenched rectangular glass plates whereby wavy crack patterns form as a result of the induced temperature gradients. The peculiar characteristic of these instabilities is that the speed of propagation is several order of magnitudes lower that the Rayleigh wave speed. Experimental studies have shown the dependence of the instabilities on certain geometrical, material, and experimental parameters (e.g. plate width, material toughness, speed of quenching). By perturbing these parameters cracks are observed to propagate along a straight line, oscillate with a periodic sinusoidal or semi-circle like morphology, or propagate in a supercritical manner. Here we formulate the problem of a propagating crack in a brittle thermoelastic material while considering the possibility of the crack undergoing bursts of supercritical crack propagation, by extending the model in? ]. We also describe a novel higher order computational framework for its numerical solution centered around Universal Meshes, Mapped Finite Element Methods, and Interaction Integral Functionals. We verify the convergence of the results and compare them against experiments. We reveal crack behaviors not previously observed. Particularly we discuss periods of sudden crack propagation, followed by temporary arrest and crack kinking. We identify various crack morphologies: sinusoidal, asymmetric, semi-circle, kinked and flattened oscillations. We investigate the frequency content of the oscillatory crack paths and study their relation to the dominating problem parameters. Additionally, we identify two new thresholds in phase space corresponding to the transition from oscillatory propagation to rapid propagation and arrest, as well as from permanent crack arrest to temporary crack arrest followed by kinking and branching.

Dedicated to Horacio Espinosa, a colleague and a friend, on the ocassion of receiving the William Prager

Medal from the Society of Engineering Science

### 1. Introduction

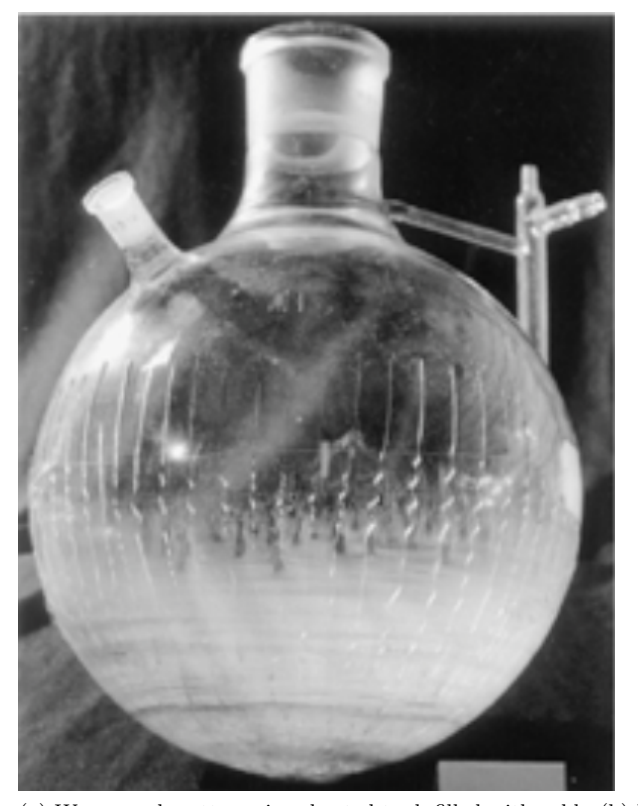
When brittle heat conductors are rapidly cooled, steep temperature gradients may induce crack propagation which, under specific environmental and geometrical conditions, may result in wavy crack formations. Some examples are the filling of heated tanks or beakers and the quenching of a glass strip as illustrated in Figs. 1(a) and 1(b), respectively.

In this manuscript we are concerned with simulating the formation of wavy crack patterns in heated amorphous, brittle plates when immersed in a cold bath. To the extent of uncovering the driving parameters of these instabilities, we simulate numerically the fracturing process and explore how variations of relevant problem parameters influence the crack path.

Since this problem has a long history, in the following we begin by briefly reviewing experimental, analytical and modeling results, followed by a detail of the contributions in this manuscript.

<sup>\*</sup>Corresponding Author

Email addresses: mchiaram@princeton.edu (Maurizio M. Chiaramonte), bponemon@stanford.edu (Benjamin E. Grossman-Ponemon), 1-keer@northwestern.edu (Leon M. Keer), 1ewa@stanford.edu (Adrian J. Lew)





(a) Wavy crack patterns in a heated tank filled with cold  $\,$  (b) Wavy crack patterns in a rapidly quenched plate [? ] fluid [? ].

Figure 1: Examples of wavy crack patterns in rapidly cooled brittle materials

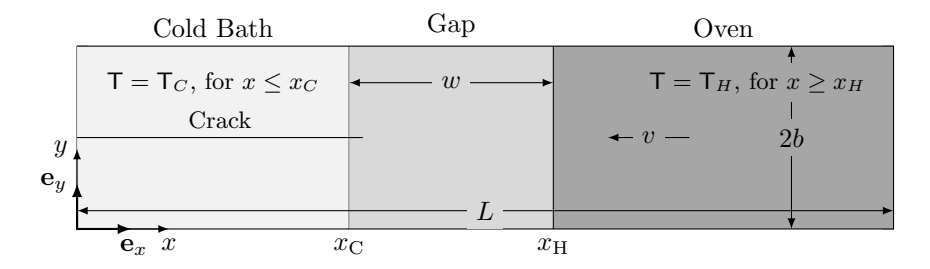


Figure 2: The schematic of the problem. We consider a plate of width 2b heated to oven temperature  $\mathsf{T}_H$  which is immersed in a bath with temperature  $\mathsf{T}_C$  ( $\mathsf{T}_C < \mathsf{T}_H$ ). The gap between the oven and the bath is given by w.

### 1.1. Experimental results

The first experimental results date back to the work of ? ] who investigated the formation of wavy cracks in a heated plate when immersed in a water bath. The phenomena was also observed by ? ] where rapidly cooling a heated flask induced the formation of wavy crack patterns (cf. Fig. 1(a)).

More recently? ? ] performed controlled experiments of a heated rectangular glass plate dipped at a velocity v in a cold bath, cf. Fig. 2 for a schematic of the test setup. The authors first investigated the crack morphology as a function of the immersion velocity v and the temperature difference  $\Delta T$  between the cold bath and the oven. Below certain values of  $\Delta T$  they noticed that the crack does not grow. When propagation occurs, they identified three types of cracks, adopting their terminology: straight, oscillatory, and branched. For oscillatory cracks, they identified three types of oscillations: sinusoidal (close to the threshold between straight and oscillatory propagation), semi-circle like (as v and  $\Delta T$  are increased), and asymmetric in the direction of propagation. Additionally, for very high speeds v, they noticed the crack growing almost entirely in the perpendicular direction to the initial crack (which coincides with the y-direction in Fig. 2) until sudden arrest. For some specimens the crack continued growing in the x-direction after forming a kink, which the authors labeled a "cusp." Also, by exploring the power spectrum of the digitized cracks, the authors noticed that for oscillatory cracks quasi-periodic or doubly periodic crack paths develop as the velocity and the temperature difference are further increased. They identified that the specimen width 2b controlled the wavelength and the amplitude of the oscillations, both through experiments and analysis, while the length L of the sample plate was reported to be unimportant. The thickness was also reported to not affect results as long as the diffusion length, defined as the ratio of the thermal diffusivity to the velocity of immersion, was much larger than the thickness.

? ] performed a similar set of experiments focusing on lower ranges of immersion velocities. The authors investigated the influence of the gap w (cf. Fig. 2) between the oven and the cold bath, the width of the plate 2b, and the temperature jump  $\Delta T$ . For a thermal profile dictated by  $(w, \Delta T, v)$  they studied the crack propagation as a function of the plate width 2b. The authors observed that for small values of  $b < b_c$  no propagation took place, for  $b_c < b < b_{osc}$  cracks propagated in the middle of the plate at a constant velocity, and for  $b > b_{osc}$  the crack path became wavy. For b values greater than  $b_{osc}$  but close to it, they noticed regular oscillations. As b was further increased, the authors observed the oscillations becoming less regular; they noted "possible period doubling, rupture of symmetry," and even crack branching for very large widths. It is worthwhile noting that the focus of the experimental study was also the transition from straight to oscillatory propagation.

? ] also performed several experiments, mostly driven by the interest in understanding the phenomenon as the crack propagates, not only from post mortem evaluation. To this extent the experimental setup was mildly altered from the one of ? ? ] and ? ] to allow the unobstructed observation of the ongoing propagation. This was achieved by moving the furnace farther away from the cooling bath. The authors examined in detail a few typical samples of the thermally quenched crack growth, showing straight, periodic oscillatory, chaotic oscillatory, and branched paths.

More recently? ] performed similar experiments, mostly focused on characterizing the stress state at the crack tip through the use of instantaneous phase-stepping photoelasticity [?]. Although their exploration of experimental parameters was not on the scale of earlier works, their contribution was in highlighting that throughout their experiments they noticed considerable variations in T-stress, as well as non-zero mode II stress intensity factors, although the crack was observed propagating smoothly.

Other similar experiments were performed by ? ] on arrays of cracks subjected to temperature gradients, as well as by ? ] on thermally loaded single-crystal silicon.

As a result of the experiments discussed, it is possible to conclude that for certain values of the controlling parameters (i.e. the cooling speed, the temperature gap, the material toughness, the plate width) the cracks may be stationary, propagate in a straight manner or undertake undulations. When the crack undertakes undulations these can be periodic, doubly-periodic or supercritical with branching. The morphology of the undulations can be sinusoidal, non-symmetric, half-circle like, or even possess cusps. The rather interesting feature of many of these regimes of propagation is that the crack advancement velocity is several orders of magnitude lower than the Rayleigh wave speed of the material, hence the fracturing process can be deemed quasi-static. Bursts of fast crack propagation speeds do appear for short crack lengths in some of these experiments, likely leading to the observed branching. Generally observed trends include that the growth of b is correlated with larger oscillation wave numbers and amplitudes, and that progressively larger instabilities

Table 1: Summary of material and geometrical parameters of the experimental investigations. Empty cells (–) indicate that the parameter was not held constant but varied throughout experiments.

Parameter	Sym.	Units	[?] <sup>†</sup>	[? ]†	[?]
Width	2b	mm	_	_	25
Young's Modulus	E	GPa	71	72	70
Poisson's Ratio	ν	_	0.23	*	*
Coeff. of Thermal Expansion	α	$10^{-6}/{ m K}$	7.7	7.7	7.7
Thermal Diffusivity	D	$\mathrm{mm}^2/\mathrm{s}$	0.47	0.47	0.47
(Plane-stress) Toughness	$K_C$	MPa √m	0.84*	0.32	0.84*
Velocity	v	mm/s	_	_	1.5
Temperature jump	ΔΤ	K	_	135	_
Non-dimensional Parameter	Sym.	Expression			
Peclet Number	P	$\frac{bv}{D}$	$\frac{bv}{0.47}~{\rm s~mm^{-2}}$	$\frac{bv}{0.47} {\rm \ s \ mm^{-2}}$	40
Non-dimensional Toughness	$\hat{K}_C$	$\frac{K_C}{\alpha E \Delta T \sqrt{b}}$	$\frac{1.5}{\Delta T \sqrt{b}} \; K \sqrt{mm}$	$\frac{4.3 \times 10^{-3}}{\sqrt{b}} \sqrt{\text{mm}}$	$\frac{0.44}{\Delta T} \text{ K}$

<sup>†</sup>**?** ], **?** ], **?** ]

are induced as  $\Delta T$  and b grow. Crack cusping (i.e. kinking) and doubly periodic oscillations of the crack path appear with further growth of this two quantities.

For later comparison of our computed crack paths with the experimental results, as well as for completeness of the review, we summarize in Table 1 the material, geometrical, and experimental parameters of the works found in [? ? ? ], alongside a description of the symbols used. Two non-dimensional quantities have been shown [? ? ? ? ] to control the behavior of the crack path: the Peclet (P) number and the non-dimensional toughness  $(\hat{K}_C)$ . The first parameter is defined as the ratio of the immersion velocity to the diffusion speed, while the second parameter is the toughness normalized by the jump in temperature and problem length scales, as shown in Table 1 and later in (10) and (11). Often, in place of the non-dimensional toughness, we will discuss the plate behavior in terms of its reciprocal value  $\hat{R} = \hat{K}_C^{-1}$ .

## 1.2. Analytical results

Considerable efforts have been invested in the analytical prediction of the instability in the works of ? ? ? ? ? ], and ? ]. The theoretical analysis of the phenomena remains an active area of research as illustrated by the relatively young literature [? ? ? ]. Most of the efforts focus on analyzing the stability of the propagating crack to identify thresholds that distinguish between no-propagation and straight propagation as well as between straight propagation and oscillatory propagation.

<sup>\*</sup>Not reported.

<sup>\*</sup>Not reported, assumed value from estimate by [?].

Arguably, the first attempt to derive the conditions under which the bifurcation from straight to oscillatory propagation takes place dates back to the work of? ]. In their analysis, rather than performing a perturbation of the crack geometry, they investigated stability through the theory of? ], treating the problem as a straight crack in an infinite plate. The stability of the crack is dictated by the developed T-stress, the zeroth order term in the expansion of the stresses about the crack tip. By finding immersion velocities for which crack propagation occurs simultaneously with tensile values of the T-stress, they identified the bifurcation points. The T-stress criterion only provided the stability of the crack path to perturbations of the crack tip, meaning that that the wavelengths of the resulting oscillations could not be quantified beyond the point of bifurcation. Additionally, for consistency with experimental results, the author proposed that the critical energy release rate be dependent on the crack speed, a proposition that was later refuted in [?].

Concurrently, ? ] also proceeded to theoretically study the transition of crack propagation from straight to oscillatory. The authors investigated the linear stability of the crack by formulating an eigenvalue problem through the linearization of the condition  $K_{II} = 0$  (also known as the Principle of Local Symmetry or PLS [?], where  $K_{II}$  is the stress intensity factor for mode II deformation). With the results of their analysis they provided threshold curves in the phase space of the Peclet number and the non-dimensional toughness (cf. [?, Fig. 3]). In their work the authors approximated the stress field with the one of an infinite plate. This may have been the root cause of discrepancies with experimental results, as the authors themselves comment.

- In [?] the authors explored the transition regions between different behaviors by performing a linear stability analysis of a crack subjected to small perturbations of its shape. The authors added a sinusoidal perturbation of amplitude A to a straight crack, and, following the principle of local symmetry, argued that for positive values of  $K_{II}/A$  the crack will follow a restoring-to-straight path, otherwise it will deviate from the straight path, or in the context of perturbations, become unstable. The transition point is found as the crack length for which  $K_{II}/A$  becomes non-positive for some perturbation frequency. The authors additionally provided results for the wavelength of the crack in the neighborhood of the transition point.
- ? ] performed an analysis founded on the dynamical law of crack propagation, proposed in [? ], reckoned as a generalization of the Principle of Local Symmetry and which allows for  $K_{II} \neq 0$  along the trajectory. Similarly to [? ], throughout the analysis the driving variable for the instabilities was the width of the specimen. By making use of the theory in [? ] they showed that the crack path, just past the instability threshold, has a stationary sinusoidal solution, and they further highlighted that propagation occurs for  $K_{II} \neq 0$ , except at specific points, from where they argued that the Principle of Local Symmetry is insufficient to determine the propagation of a crack.

More recently? ] performed a theoretical analysis of the trajectory of the crack without resorting to the infinite plate approximation and without restricting the crack tip to lie along the centerline of the sample, in addition to numerical simulations discussed in §1.3. The authors relied on Griffith's theory and the PLS in their predictions of thresholds in phase space.

In an effort to unify all available theoretical results, we reproduced (through common normalization) a recollection of the theoretically derived thresholds for the different crack regimes of the authors in [???]. This is shown in Fig. 3. These theories remain confined to the critical state at the transition from straight to oscillatory paths. This limitation thus demands for exploratory tools, such as numerical analyses, for broader investigation of the phase space of crack behaviors.

#### 1.3. Numerical simulations

Studies based upon numerical simulations include the works of ????????.

Arguably, ? ] was the first to simulate the development of oscillations with finite element methods. The simulations were restricted to small amplitudes given that a conforming mesh was generated by mapping an initial mesh. In the simulations, the authors first advanced the position of the cooling front at a fixed crack tip position, and subsequentially, at a fixed position of the cooling front, they advanced the crack tip position until configurational force balance was attained.

- ? ] studied the problem using plane-stress, finite strain elastodynamics. The authors' employed cohesive zone elements within the framework of finite element methods (cf. [? ]) to simulate the development of oscillatory paths and even crack branching. Although oscillations appeared in the simulations, the computed crack paths showed considerable influence of the chosen spatial discretization.
- ? ] performed several simulations of a rectangular plate whose top and bottom boundaries (parallel to the longitudinal axis) were constrained against normal movement. The temperature field was taken to be

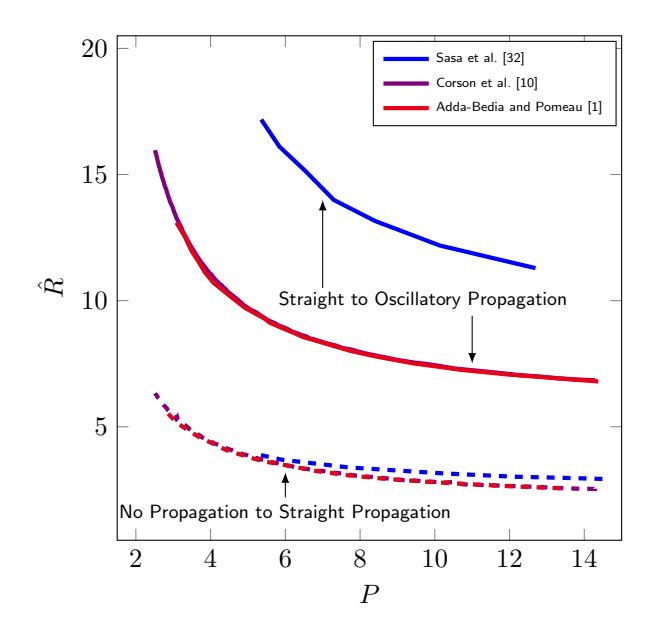


Figure 3: Comparison of analytical transition thresholds from no propagation to straight propagation (dashed curves) and straight to oscillatory propagation (solid curves). The above curves are reproduced by digitizing the corresponding images in ? ], ? ], and ? ]. The curves of [? ] and [? ] are nearly indistinguishable.

discontinuous at the interface between the cold bath and the air. The crack was advanced in accordance with Griffith criterion and the Principle of Local Symmetry. Their control parameters were the toughness of the material as well as the temperature jump. A total of ten unique simulations (in terms of the pairing of toughness and jump in temperature) were performed which resulted in five unique values of the non-dimensional toughness. As they imposed a discontinuous temperature field, the additional dependence on the diffusion length vanished, or effectively the Peclet number was taken to infinity. With the five unique values of the non-dimensional toughness, they provided ranges for qualitative cracks behaviors being straight, wavy, wavy with increased amplitude, and sharp crack turning and arrest.

? ], alongside experimental observations, simulated the crack evolution using boundary element methods previously described in [? ? ]. The direction of crack propagation was chosen by the authors according to the Maximum Tangential Stress criterion of ? ]. In their simulations the authors were the first to highlight the presence of configurationally unstable crack propagation, in qualitative agreement with experimental results. Additionally, the authors were able to confirm through their numerical experiments that the stability criterion of ? ] employed by ? ] was insufficient to capture the primary bifurcation, a conjecture previously discussed in ? ? ? ].

In [?] the authors simulated the crack propagation via the phase field model of ?]. The simulations focused on predicting the threshold of the instability as well as the nature of the oscillations in the close proximity to the threshold. As the authors remark, their computational framework fell short of replicating the complex paths observed experimentally in [?] for control parameters well above the threshold between straight and oscillatory crack propagation.

? ] also employed a form of regularization by exploiting the peridynamic framework to account for the evolving fracture. The authors simulated crack branching, and even the development of multiple cracks from the edge of the quenched plate.

In ? ] the authors performed similar analysis with an elastodynamic X-FEM formulation. Notably, they defined the crack tip velocity to be a function of the energy release rate, from dynamic fracture, and used the Principle of Local Symmetry (which they compared with the maximum hoop stress criterion) for fracture propagation. Similarly to ? ], elastic waves were slowed down by artificially increasing the mass density to attain a larger critical time step in explicit dynamics, and the waves were quickly dissipated through artificial viscosity. Thus, if there were any dynamic effects that affected the potential direction of propagation, they were not necessarily captured. This is an interesting perspective over previous works, since as we shall show here as well, the crack may propagate with  $K_I > K_C$  over finite lengths even in the quasi-static setting; see

the discussion in §1.4.

Additional contributions that should be cited, albeit not directly correlated to the current study, are the work of? ] and? ], with the former being an observation of oscillatory propagation through a particle lattice subjected to inhomogeneous boundary conditions, and the latter being a numerical study with mass-spring systems through a two dimensional crystal.

Seldom evidence of numerical convergence (with the exception of the work of ? ]) was shown in the mentioned numerical studies. It was our experience that the appearance of oscillations was far from being indicative of converged solutions and, as discussed in §4, we will showcase the converged behavior of the results of the simulations herein.

### 1.4. Contributions

In this manuscript we formulate the problem of a propagating crack in a brittle thermoelastic material while considering the possibility of the crack undergoing bursts of supercritical crack propagation, during which  $K_I > K_C$  for short but finite crack propagation lengths, as highlighted in the observations by ? ] and illustrated later in this manuscript. To this end, we extend the model for crack propagation of ? ] to curvilinear cracks that may kink, which retains the quasi-static description of the stress field, allows for the appearance of supercritical cracks, and reduces to Griffith's model for critically-loaded cracks. In this model, supercritical cracks advance a finite length in an inifinitesimal time interval, tracing a curvilinear trajectory along the way. The crack length is therefore discontinuous in time. In all cases, even for supercritical bursts, we adopt the Principle of Local Symmetry (PLS) [?] to determine the direction of propagation.

We rewrite the model by ? ] in a distinctive way: the unknowns are arbitrary parameterizations of the crack length and time. This introduces a gauge, due to the freedom to reparameterize, and enables the crack length, time, and stress intensity factors to be continuous functions of the new parameter even in regions of crack arrest or supercritical growth. An interesting outcome of introducing this parameterization is that it is possible to formulate a discrete crack evolution algorithm in a natural way, recovering in this way a known algorithm used in the literature (e.g. [?]) which we adopt herein.

We then proceed to discretize the problem and provide a brief description of a novel computational toolset [?] for the simulation of the propagating crack capable of obtaining converged solutions of this phenomenon in a rather computationally inexpensive manner. The framework is based upon the use of Universal Meshes [?], Mapped Finite Element Methods [?], and an extension to thermoelastic problems of the formulation of the Interaction Integrals found in [?]. What make this computational framework special are that: (a) the mesh for each crack snapshots is automatically obtained without user intervention, and (b) stress intensity factors values are computed with fourth order of convergence in the mesh size at each crack tip position. The latter enables us to observe convergence of the crack path without the need to refine the mesh around the crack tip at each loading step. It also significantly lowers the computational cost of obtaining converged crack paths. We extensively verified the convergence of the obtained crack paths, and hence we are confident that the crack paths solutions we present in this manuscript are very close to the exact mathematical solutions of the model.

The light nature of the computational framework allowed us to undertake a large parametric exploration in §4, in which we were able to compare the results against previous analytical and experimental work, and interestingly, also identify crack propagation regimes not previously observed. Amongst them we identified two new thresholds in phase space: the transition from oscillatory propagation to rapid propagation and arrest, which we term snap back due to their shape, and from permanent crack arrest to temporary crack arrest followed by kinking and branching. We also identified different crack path morphologies in the oscillatory regime (wave-like, semi-circular, flattened oscillations, and kinked oscillations), and highlighted the evolution of crack speeds. Additionally, we were able to capture the frequency content observed in experiments of the oscillatory cracks, including the appearance of a double period of oscillation. We also identified periods of supercritical propagation, arising after crack arrest, mode-mixity change, and then kinking. Finally, we propose a novel methodology based on? 's prediction of crack speed [?] and on? 's criterion [?] for the prediction of the onset of crack branching, which agrees remarkably well with the experimental results of? ]. This seems to be the first time a threshold for branching has been numerically identified in phase space. Thus, the numerical results in this manuscript venture well past the primary bifurcation from straight to oscillatory propagation, capturing propagation regimes as well as crack morphologies previously not observed in numerical simulations.

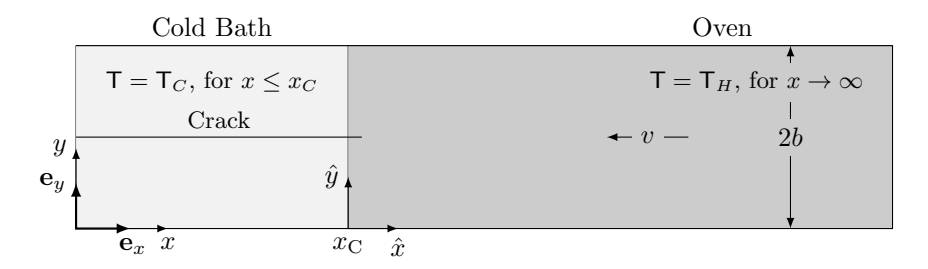


Figure 4: The schematic of the problem assuming  $w \gg \ell_D$ .

Organization. In  $\S 2$  we introduce the physical problem and its mathematical description, and in  $\S 3$  its numerical discretization. The examination of the computed results is presented in  $\S 4$ . Conclusions are stated in  $\S 5$ .

### 2. Problem Statement

The problem consists of a through crack propagating in a constant thickness (much smaller than any other dimension) rectangular plate of width 2b and length L. The plate is being submerged at velocity v in an ice-bath of temperature  $\mathsf{T}_C$  after being passed through an oven at temperature  $\mathsf{T}_H$ . The distance between the ice bath and the oven is denoted by w. Refer to Fig. 2 for a schematic of the problem.

The immersion process is assumed to be sufficiently slow such that inertial effects can be neglected, and hence we treat the solid deformation as quasi-static. This assumption is likely violated after crack kinks, in which the mode I stress intensity factor along the direction of crack propagation may grow strictly larger than the material toughness, and hence the crack propagates very fast during a very short time interval. Within the quasi-static approximation, this fast propagation is manifested as the crack advancing at infinite speed, i.e., the crack advances a finite distance in an infinitesimal time interval. These short bursts of crack advancement will be termed *supercritical crack propagation*. The potential appearance of supercritical crack propagation prompts two special considerations in the formulation of the model: (a) the parameterization of the evolution with a parameter other than time, and (b) the formulation of a model for supercritical crack propagation. Both are detailed next.

Assuming a priori that the crack does not bifurcate, the crack path will be parameterized by a continuous curve  $\mathscr{C}: [0, +\infty) \to \mathbb{R}^2$ ,  $\mathscr{C}(\xi)$ . Both the arclength of the crack a and time t will be parameterized by continuous, non-decreasing functions  $a(\xi)$  and  $t(\xi)$ , for  $\xi \in [\xi_0, +\infty)$ , for some  $\xi_0 > 0$ . The motivations behind this special parameterization are twofold, see Fig. 6 later in this section. It is not possible to adopt the crack length to parameterize the evolution because the crack may arrest, in which case a is constant but t is not. Conversely, it is not possible to parameterize by time because during supercritical crack propagation t is constant but a is not.

In the following, the onset of crack growth is defined by Griffith's criterion, and the direction of evolution is defined by the PLS. During supercritical crack propagation, Griffith's criterion will not be satisfied, since the mode I stress intensity factor along the direction of propagation will be larger than the toughness, but PLS will still be enforced. This is effectively the simplest extension of the quasi-static model to the supercritical regime.

Towards formulating the equations that describe the model, let  $\Omega = (0, L) \times (0, 2b)$  denote the domain occupied by the plate, and let x-y be a set of Cartesian coordinates fixed to the plate with associated othonormal basis  $\mathbf{e}_x$ ,  $\mathbf{e}_y$ . It will also be convenient to define a moving set of coordinates  $\hat{x} = x - vt$  and  $\hat{y} = y$ , in which the temperature field will be stationary. We choose  $\hat{x} = 0$  to coincide with the position of the cold front,  $x_C$ .

The thermal model is built based on a few simplifying assumptions. A linear thermoelastic constitutive behavior is adopted, and the effects of mechanical deformations on the energy balance are neglected. It is assumed that heat is allowed to flow freely across the faces of the crack, and that no heat exchange takes place with the surrounding air. Let  $\ell_D = D/v$  be the diffusion length, where D is the thermal diffusivity. Then, if additionally  $w \gg \ell_D$  (as it is the case for the experiments in [? ? ]), it is possible to ignore the gap between the oven and the cold front and assume that the oven is placed at an infinite distance from the

bath  $(x_H \to \infty)$ ; c.f. Figs. 2 and 4. Furthermore, only situations in which the cold front  $x_C$  is at least a few diffusion lengths from the right end of the plate x = L will be considered, so it is possible to replace the finite length of the plate for an infinitely long one. Finally, the temperature field  $\mathsf{T}(x,y,t)$  is assumed: (a) to be steady in the moving  $\hat{x}$ - $\hat{y}$  frame, and hence we may write  $\mathsf{T}(x,y,t) = \Delta \hat{\mathsf{T}}(x-vt,y) + \mathsf{T}_H$ , for a function  $\Delta \hat{\mathsf{T}} \colon \mathbb{R} \times (0,2b) \to \mathbb{R}$ ,  $\Delta \hat{\mathsf{T}}(\hat{x},\hat{y})$ , of  $\hat{x}$  and  $\hat{y}$  only, and not time, and (b) equal to the temperature jump of the bath once inside it (instantaneous cooling), and hence  $\Delta \hat{\mathsf{T}}(\hat{x},\hat{y}) = \mathsf{T}_C - \mathsf{T}_H$  for  $\hat{x} \leq \hat{x}_C = 0$ , where  $\hat{x}_C = 0$  is the  $\hat{x}$  coordinate indicating the position of the cold front. In the unsubmerged portion of the domain  $\hat{x} > 0$ , the thermal problem that defines the temperature field  $\mathsf{T}(x,y,t)$  then reads:

**Problem 2.1.** Find  $\Delta \hat{\mathsf{T}} \in H^1((0,+\infty) \times (0,2b); \mathbb{R})$  such that  $\Delta \hat{\mathsf{T}}(0,\hat{y}) = \mathsf{T}_C - \mathsf{T}_H$ ,  $\lim_{\hat{x}\to\infty} \Delta \hat{\mathsf{T}}(\hat{x},\hat{y}) = 0$  for all  $\hat{y} \in (0,2b)$ , and

$$\frac{\partial \Delta \hat{\mathsf{T}}}{\partial \hat{x}} + \frac{D}{v} \operatorname{div} \operatorname{grad} \Delta \hat{\mathsf{T}} = 0, \quad in \ (0, +\infty) \times (0, 2b),$$

$$\operatorname{grad} \hat{\mathsf{T}} \mathbf{n} = 0, \quad on \ \hat{y} \in \{0, 2b\}.$$
(1)

The temperature field over  $\Omega$  is computed as  $\mathsf{T}(x,y,t) = \Delta \hat{\mathsf{T}}(x-vt,y) + \mathsf{T}_H$  for each t.

We note that the advection-diffusion equation (1) results from transforming the standard heat equation into the moving  $\hat{x}$ - $\hat{y}$  frame under assumption (a) above. A similar thermal model has been adopted in [?], in which the authors favorably compared the results of this model with those stemming from a two-dimensional numerical computation.

The mechanical fields can be defined next. Given a crack set  $\Gamma \subset \Omega$  such that  $\Omega \setminus \Gamma$  is a connected domain, and a temperature field  $T: \Omega \to \mathbb{R}$ , the displacement field u in the x-y frame is the solution of the following problem:

**Problem 2.2.** Find  $\mathbf{u} \in \mathcal{V}_{\mathbf{u}} = \{ \mathbf{v} \in H^1(\Omega \setminus \Gamma; \mathbb{R}^2) \mid \mathbf{v} \cdot \mathbf{e}_x = \mathbf{0} \text{ at } x = L \}$  such that

$$\int_{\Omega \setminus \Gamma} \boldsymbol{\sigma}(\operatorname{grad} \boldsymbol{u}, \mathsf{T}) \colon \nabla \mathbf{v} \ d\Omega = 0$$
 (2)

for all  $\mathbf{v} \in \mathcal{V}_{\boldsymbol{u}}$ , where

 $\sigma(\operatorname{grad} u, \mathsf{T}) = \mathbb{C} : \operatorname{grad} u + \zeta \mathsf{T} 1.$ 

Here

$$\mathbb{C} = \hat{\lambda} \mathbf{1} \otimes \mathbf{1} + 2\mu \mathbb{I}, \quad \hat{\lambda} = \frac{2\lambda\mu}{\lambda + 2\mu}, \quad \zeta = -\frac{2\mu(3\lambda + 2\mu)}{\lambda + 2\mu}\alpha,$$

where  $\lambda$  and  $\mu$  are Lamé's first and second parameters, respectively,  $\hat{\lambda}$  is the modified  $\lambda$  modulus for plane stress,  $\alpha$  is the linear coefficient of thermal expansion, and  $\mathbf{1}$  and  $\mathbb{I}$  are the second-order identity and the fourth-order symmetric identity operators, respectively.

The prescribed boundary condition in Problem 2.2 approximates the effect of the device holding the glass plate (see the experimental setup of [?]). One more condition is needed to constrain rigid translations along the y-direction and to uniquely define a solution. Such condition could take the form of  $\int_0^{2b} \mathbf{v}(L,y) \cdot \mathbf{e}_y \ dy = 0$ , or in the finite element discretization later, as simply fixing the position of a node at the right end of the plate. The displacement field that solves Problem 2.2 is defined once  $(\mathsf{T},\Gamma)$  is prescribed, a dependence indicated as  $u[\mathsf{T},\Gamma]$ .

To compute the evolution of the crack, it is necessary to introduce the stress intensity factors (SIFs). Given a crack set  $\Gamma$  and a temperature field  $\mathsf{T}$ , the SIFs at a crack tip  $x_{\mathsf{T}} \in \Gamma$  can be defined as

$$K_{I}[\Gamma, \boldsymbol{x}_{\top}, \mathsf{T}] = \lim_{r \searrow 0} \sqrt{r} \, \boldsymbol{\sigma}(\operatorname{grad} \boldsymbol{u}[\mathsf{T}, \Gamma], \mathsf{T}) : \mathbf{e}_{\vartheta} \otimes \mathbf{e}_{\vartheta} \Big|_{\vartheta = 0}$$
(3a)

$$K_{II}[\Gamma, \boldsymbol{x}_{\top}, \mathsf{T}] = \lim_{r \searrow 0} \sqrt{r} \, \boldsymbol{\sigma}(\operatorname{grad} \boldsymbol{u}[\mathsf{T}, \Gamma], \mathsf{T}) : \mathbf{e}_{\vartheta} \otimes \mathbf{e}_{r} \big|_{\vartheta = 0}$$
(3b)

where  $(r, \vartheta)$  and  $\{\mathbf{e}_r, \mathbf{e}_{\vartheta}\}$  are the set of polar coordinates and polar basis at  $\boldsymbol{x}_{\top}$ , respectively, which depend on  $\boldsymbol{x}_{\top}$  and the tangent to  $\Gamma$  at  $\boldsymbol{x}_{\top}$  for their definition, see Fig. 5(a).



(a) The local crack tip polar coordinates. Points with  $\vartheta = 0$  lie on a line tangent to the crack at the crack tip (see dashed line).

(b) The kinked extension of a crack.

Figure 5: Crack tip coordinates and kinked extension.

For cracks with the potential for kinks to appear, the relevant SIFs are  $K_I^+$  and  $K_{II}^+$ . These are the SIFs that would arise as a result of adding an infinitesimal kink to the crack tip (cf. ? ]). To this end, consider the kink-extended crack set

$$\Gamma_{\text{kinked}}(\Gamma, \boldsymbol{x}_{\top}, \mathsf{v}) = \Gamma \cup \{\boldsymbol{x}_{\top} + \zeta \mathsf{v} \mid \zeta \in [0, 1]\} \tag{4}$$

for  $v \in \mathbb{R}^2$ , which joins  $x_{\top}$  to the crack tip  $x_{\top} + v$  of the kink-extended crack, see Fig. 5(b). The stress intensity factors of interest are then defined as

$$K_I^+[\Gamma, \boldsymbol{x}_\top, \mathsf{T}, \mathsf{k}] = \lim_{\epsilon \searrow 0} K_I[\Gamma_{\text{kinked}}(\Gamma, \boldsymbol{x}_\top, \epsilon \mathsf{k}), \boldsymbol{x}_\top + \epsilon \mathsf{k}, \mathsf{T}]$$
(5a)

$$K_{I}^{+}[\Gamma, \boldsymbol{x}_{\top}, \mathsf{T}, \mathsf{k}] = \lim_{\epsilon \searrow 0} K_{I}[\Gamma_{\text{kinked}}(\Gamma, \boldsymbol{x}_{\top}, \epsilon \mathsf{k}), \boldsymbol{x}_{\top} + \epsilon \mathsf{k}, \mathsf{T}]$$

$$K_{II}^{+}[\Gamma, \boldsymbol{x}_{\top}, \mathsf{T}, \mathsf{k}] = \lim_{\epsilon \searrow 0} K_{II}[\Gamma_{\text{kinked}}(\Gamma, \boldsymbol{x}_{\top}, \epsilon \mathsf{k}), \boldsymbol{x}_{\top} + \epsilon \mathsf{k}, \mathsf{T}]$$
(5a)

where  $k \in \mathbb{R}^2$ , ||k|| = 1, is a unit vector indicating the direction of the infinitesimal kink.

The problem that defines the evolution of the crack then reads:

**Problem 2.3.** Let  $\mathscr{C}([0,\xi_0]) \subset \Omega$  for  $\xi_0 > 0$  be the given initial crack, such that  $\mathscr{C}(\xi_0) \neq \mathscr{C}(0) \in \Omega$ , and let  $T(t) \equiv T(\cdot,\cdot,t)$  denote the temperature field solution of Problem 2.1 at time t. Find the crack path  $\mathscr{C}: [0,\infty) \to \mathbb{R}^2$ , the arclength  $a: [\xi_0,\infty) \to \mathbb{R}$ ,  $a(\xi_0) = a_0 > 0$ , the time parameterization  $t: [\xi_0,+\infty) \to \mathbb{R}$ ,  $t(\xi_0) = 0$ , and the kink direction  $k: [\xi_0, +\infty) \to \mathbb{R}^2$ ,  $||\mathbf{k}|| = 1$ , so that for almost every  $\xi \in [\xi_0, \infty)$ 

$$a'(\xi) (K_C - K_I^+(\xi, \mathsf{k}(\xi))) \le 0, \qquad a'(\xi) \ge 0,$$
 (6a)

$$t'(\xi) (K_C - K_I^+(\xi, k(\xi))) \ge 0,$$
  $t'(\xi) \ge 0,$  (6b)

$$K_{II}^{+}(\xi, \mathsf{k}(\xi)) = 0, \tag{6c}$$

$$\mathscr{C}'(\xi) = a'(\xi)\mathsf{k}(\xi). \tag{6d}$$

where, abusing notation,

$$\begin{split} K_I^+(\xi,\mathbf{k}(\xi)) &= K_I^+\left[\mathcal{C}([0,\xi]),\mathcal{C}(\xi),\mathsf{T}(t(\xi)),\mathbf{k}(\xi)\right],\\ K_{II}^+(\xi,\mathbf{k}(\xi)) &= K_{II}^+\left[\mathcal{C}([0,\xi]),\mathcal{C}(\xi),\mathsf{T}(t(\xi)),\mathbf{k}(\xi)\right]. \end{split}$$

In this problem we assume that the crack tip  $\mathscr{C}(\xi)$  never reaches the boundary of the plate.

A few words about this evolution are now appropriate. For the forthcoming discussion I will denote an open interval in  $\mathbb{R}$ . The model by ? ] is restated in (6a) and (6b), here in terms of the arbitrary parameterization of t and a as well as in terms of the unknown kink direction k. It is simple to see that any reparameterization of a, t, k with  $\xi(\zeta)$  for  $\zeta \in [\zeta_0, +\infty), \xi'(\zeta) \geq 0$ , also satisfies the same equations. The value of  $k(\xi)$  is determined by (6c), or the PLS condition. There will generally exist only one direction  $k(\xi)$ defined by this equation (see, e.g., [?] for a discussion), but there could be more. In particular, if the stress intensity factors are identically zero, then any direction k will be a solution, as in the perfectly unstressed case. For a smooth enough curve  $\mathscr{C}$  (e.g. Lipschitz continuous), its length is computed as

$$a(\xi) = \int_0^{\xi} \|\mathscr{C}'(\xi)\| d\xi \tag{7}$$

for any  $\xi \in [0, +\infty)$ . This relationship is enforced through (6d).

Notice that, from (6a), when  $K_C - K_I^+(\xi, \mathsf{k}(\xi)) > 0$  for  $\xi \in I$ , necessarily  $a'(\xi) = 0$  in I, which corresponds to crack arrest. At the same time, from (6b),  $t'(\xi)$  can take any non-negative value in I. Since the temperature field changes only when  $t(\xi)$  does, selecting  $t'(\xi) = 0$  in this case will advance neither the crack nor time. This is a result of the freedom to parameterize time that comes with this formulation. If desired, to uniquely define the evolution of time a condition such as  $t'(\xi) = 1$  when  $K_C - K_I^+(\xi, \mathsf{k}(\xi)) > 0$  could be imposed. However, this would not change any of the physically meaningful quantities, namely, the time evolution of the temperature field, the displacement field, or the crack path.

Supercritical propagation is obtained when  $K_C - K_I^+(\xi, \mathsf{k}(\xi)) < 0$  for  $\xi \in I$ , and in this case  $a'(\xi) \geq 0$  but  $t'(\xi) = 0$  for  $\xi \in I$ . Therefore, under these conditions the crack may propagate a finite distance at constant time, as alluded to earlier. Setting  $a'(\xi) = 0$  for  $\xi \in I$  freezes the evolution of both time and the crack path, reflecting again the freedom to choose the parameterization of the crack path in this formulation. If desired, a condition such as  $a'(\xi) = 1$  when  $K_C - K_I^+(\xi, \mathsf{k}(\xi)) < 0$  could be imposed to uniquely define the crack path  $\mathscr C$  without changing any of the physically meaningful quantities.

If  $K_C - K_I^+(\xi, k(\xi)) = 0$  for  $\xi \in I$ , the classical case of quasi-static crack propagation is recovered, provided that  $t'(\xi) > 0$  whenever  $a'(\xi) > 0$  in I. In this case both  $a'(\xi)$  and  $t'(\xi)$  need only be non-negative, so it is possible to have  $t'(\xi) = a'(\xi) = 0$  for  $\xi \in I$ . This can again be interpreted as an artifact of the unprescribed parameterization of either function, and hence can be remediated. So, is there really a choice of  $t'(\xi) > 0$  and  $a'(\xi) > 0$ , or should their values be related in some way? The simplest way to think about this case is by resorting to a discretization in  $\xi$ , which is also useful for the upcoming numerical approximation. Assume that t'>0 in some neighborhood of  $\xi$ . Then  $t(\xi)< t(\xi+\Delta\xi)$  for some  $\Delta\xi>0$ small enough, and thus  $\mathsf{T}(t(\xi+\Delta\xi))\neq\mathsf{T}(t(\xi))$ . Insisting on a'=0 in the same neighborhood of  $\xi$  means that the crack does not grow. However, the stress field is changing with  $\xi$ , since T is, and such stress field should be such that (6c) and  $K_C - K_I^+(\xi + \Delta \xi, k(\xi + \Delta \xi)) = 0$ . Apart from exceptional circumstances, the problem is overconstrained, and the way to satisfy the last two equations is to let the crack grow, or a'>0 in a neighborhood of  $\xi$ . An analog argument can be made if instead the assumption is that  $a'(\xi)>0$ and t'=0 in some neighborhood of  $\xi$ . In this case, the stress field, and hence the stress intensity factors, would change due to the growth of the crack in lieu of the temperature field, and the only way to satisfy the equations is by adjusting the value of t'. Therefore, in general, the values of  $a'(\xi)$  and  $t'(\xi)$  are related to each other upon quasi-static crack propagation.

There are three more interesting observations about the model. First, irreversibility of crack propagation is enforced by the fact that  $\mathscr{C}([0,\xi_1])\subseteq\mathscr{C}([0,\xi_2])$  if  $\xi_1<\xi_2$ . Second, a novel feature of this model is (6d), which enables k to indicate directions of potential propagation, but along which the crack may not propagate if (6a) requires  $a'(\xi)=0$ . Third, even though the tangent vector to the crack set is discontinuous at kinks, the stress intensity factors  $K_I^+(\xi,\mathsf{k}(\xi))$  and  $K_{II}^+(\xi,\mathsf{k}(\xi))$ , and the kink direction  $\mathsf{k}(\xi)$ , will generally be continuous functions of  $\xi$  if the temperature field  $\mathsf{T}(\xi)$  is. The numerical simulations later suggest that this is the case.

The extension of the quasi-static model to the propagation of supercritical cracks is expected to be accurate for cracks in which  $K_I^+ - K_C \ll K_C$ , or cracks in which the fraction of the elastic energy release rate that might be converted to kinetic energy is very small in relation to the surface energy per unit length. The simple calculation in [?, c.f. §4.1] suggests that the speed of the crack should be about one-third of the dilatational wave speed for inertial effects to affect the structure of the crack tip fields. An alternative way of thinking about the model herein is as being valid when the sound speeds of the material are large enough or the mass density small enough. Colloquially speaking, in this case the elastic fields have a chance to equilibrate before the crack can further grow. As we shall see, these assumptions are violated as the Peclet number grows or the non-dimensional toughness decreases, and branching is experimentally observed.

#### 3. Problem Solution

We introduce next the (numerical/analytical) solutions of Problems 2.1, 2.2, 2.3. For clarity of presentation we provide only an overview of the crack propagation algorithm, which we will discuss elsewhere.

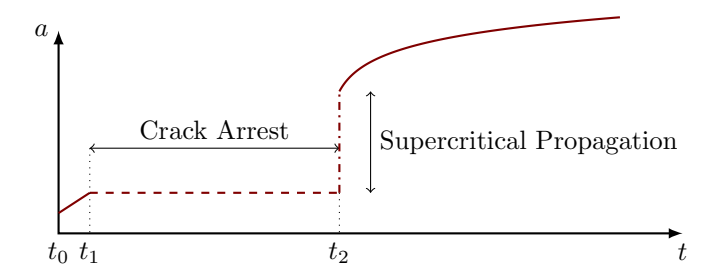


Figure 6: The propagation regimes of a crack. The crack may propagate in such a way that the crack length a is a function of time t (eg.  $t_0 \le t < t_2$  and  $t > t_2$ ), in such cases crack propagation is stable. When a can be expressed as a constant in time we observe crack arrest (eg.  $t_1 \le t < t_2$ ). At certain times the crack length may not be expressed as a function of time and at those times we expect supercritical crack propagation (eg.  $t = t_2$ ). As supercritical crack propagation is allowed as part of the model here, it becomes apparent that crack length may not be parameterized by time.

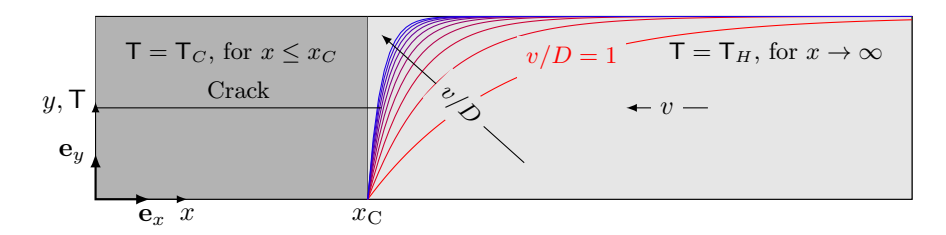


Figure 7: The modeled problem with the temperature distribution for a range of ratios of v/D. The larger the value, the steeper the temperature field becomes.

#### 3.1. The Thermal Problem

The solution to Problem 2.1 can be found in closed form, and it is

$$\Delta \hat{\mathsf{T}}(\hat{x}, \hat{y}) = -\exp\left(-\frac{v\hat{x}}{D}\right) H(\hat{x}) \Delta \mathsf{T} \tag{8}$$

where H denotes the Heaviside function  $(H(\hat{x}) = 1 \text{ if } \hat{x} \ge 0, \text{ and } 0 \text{ otherwise})$  and  $\Delta \mathsf{T} = \mathsf{T}_H - \mathsf{T}_C$ . This implies that

$$\mathsf{T}(x,y,t) = \left\{ 1 - \exp\left[-\frac{v(x-vt)}{D}\right] \right\} \ H(x-vt) \ \Delta \mathsf{T} + \mathsf{T}_C \tag{9}$$

Fig. 7 showcases the problem geometry, as well as the temperature distribution for several values of the ratio v/D.

### 3.2. The Mechanical Problem

Given a crack set  $\Gamma$  and temperature field  $\Gamma$ , the displacement field  $u[\Gamma, T]$  which solves Problem 2.2 is approximated by employing a variant of the Finite Element Method, the Mapped Finite Element Method (MFEM) introduced in [?]. We term the approximate solution  $u^h$ . MFEM addresses the singular nature of the displacement field around the crack tip, recovering optimal rates of convergence for singular elasticity solutions, and hence renders higher-order approximations of the stress field. The higher order will prove pivotal in allowing the evaluation of essentially converged approximations for modest computational expenditures. In particular, higher-order approximations circumvent the need to construct refined meshes in the neighborhood of each discrete position of the crack tip. Essentially the same mesh is used throughout the computation of the entire crack path, except for regions in which the geometric features of the path (i.e. kinks) require a smaller mesh size for their representation.

## 3.3. The Evaluation of the Stress Intensity Factors

The calculation of the Stress Intensity Factors (SIFs) is carried out by employing a similar formulation of Interaction Integrals introduced in [?]. We recall that the interaction integral  $\mathcal{I}[\cdot,\cdot]$  is a bilinear functional of

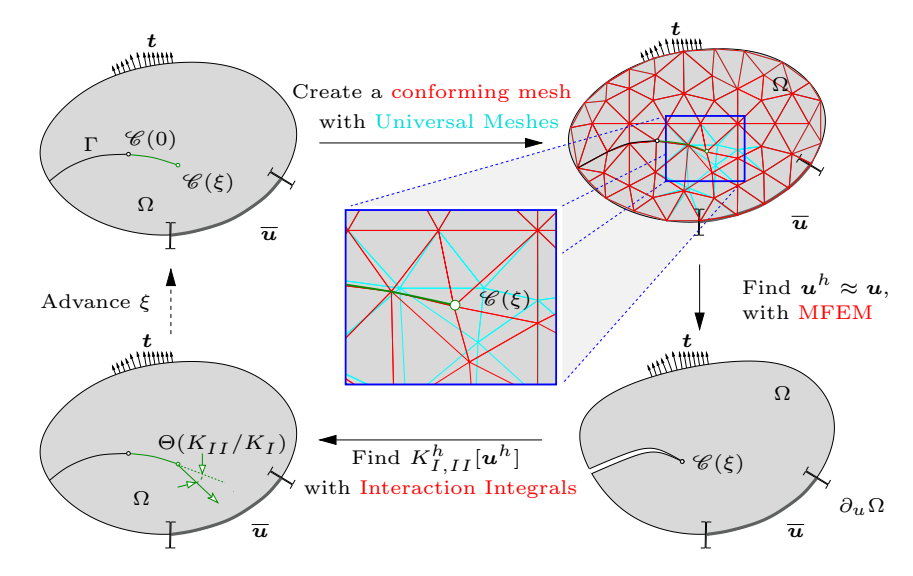


Figure 8: Schematic of propagation algorithm. The detail at the center shows the undeformed Universal Mesh in cyan over the reference configuration. The deformed mesh that conforms to the crack geometry is shown in red. The figure at the bottom-right shows the deformed configuration computed with MFEM.

two tensor fields  $\beta^a$  and  $\beta^b$  (interpreted as gradients of displacement fields) whose value satisfies the relation

$$I[\boldsymbol{\beta}^a, \boldsymbol{\beta}^b] = \eta \left( K_I[\boldsymbol{\beta}^a] K_I[\boldsymbol{\beta}^b] + K_{II}[\boldsymbol{\beta}^a] K_{II}[\boldsymbol{\beta}^b] \right),$$

where  $K_{I,II}[\boldsymbol{\beta}^{a,b}]$  are the stress intensity factors for mode I,II for each of the tensor fields. Thus, setting  $\boldsymbol{\beta}^a := \operatorname{grad} \boldsymbol{u}$ , its stress intensity factors are evaluated by crafting two tensor fields  $\boldsymbol{\beta}_i^{\operatorname{aux}}$ ,  $i \in \{I,II\}$ , which satisfy  $K_i[\boldsymbol{\beta}_j^{\operatorname{aux}}] = \delta_{ij}$ ,  $i,j \in \{I,II\}$ , and setting  $\boldsymbol{\beta}^b \in \{\boldsymbol{\beta}_I^{\operatorname{aux}}, \boldsymbol{\beta}_{II}^{\operatorname{aux}}\}$ . For more details we refer the reader to [?].

The interaction integrals found in [?] are extended to account for the dependence of the SIFs on the temperature; their precise form and a derivation are provided in Appendix A.

### 3.4. Crack Propagation Algorithm

The crack propagation algorithm to integrate the model introduced here is discussed in detail in [?]. In the following, we present its salient features.

The algorithm integrates the crack evolution in  $\xi$ . Let  $\xi_0 < \xi_1 < \ldots < \xi_m$  be a partition of  $[\xi_0, \xi_m]$ , and choose  $\Delta t > 0$  and  $\Delta a > 0$ . Also, denote by  $t_n$ ,  $a_n$ , and  $k_n$  the approximations to  $t(\xi_n)$ ,  $a(\xi_n)$ , and  $k(\xi_n)$ , respectively. Finally, let  $\mathbf{e}_r$  and  $\mathbf{e}_\vartheta$  be the polar basis at the crack tip  $\mathscr{C}(\xi_n)$ , and let  $\Gamma_n = \mathscr{C}([0,\xi_n])$  be the crack set at  $\xi_n$ . The time integration and crack propagation scheme consists of four simple steps (c.f. Fig. 8). At  $\xi = \xi_n$ :

- i. Generate a conforming subdivision to  $\Omega \setminus \Gamma_n$  with *Universal Meshes* [?].
- ii. Find an approximation of the displacement field  $\boldsymbol{u}[\Gamma_n,\mathsf{T}(t_n)]$ , generated by the temperature field  $\mathsf{T}(t_n)$  with MFEM [?].
- iii. Evaluate the stress intensity factors  $K_{jn} = K_j[\Gamma_n, \mathscr{C}(\xi_n), \mathsf{T}(t_n)]$ , for j = I, II, with Interaction Integral Functionals [?] adapted as in §3.3.
- iv. Define  $\mathsf{k}_n = \mathbf{e}_r(\Theta_n)$  as the unit vector that forms an angle

$$\Theta_n = \Theta(K_{IIn}/K_{In}) = 2 \arctan \left[ \frac{-2K_{IIn}/K_{In}}{1 + \sqrt{1 + 8(K_{IIn}/K_{In})^2}} \right]$$

from the crack tip tangent direction (see Fig. 5(b)). Compute  $K_{In}^+ = \text{sign}(K_{In}) \sqrt{K_{In}^2 + K_{IIn}^2}$ . Then,

```
a if K_{In}^+ < K_C advance time t_{n+1} = t_n + \Delta t and keep a_{n+1} = a_n.
b else if K_{In}^+ \ge K_C propagate the crack a_{n+1} = a_n + \Delta a in the direction of k_n and keep t_{n+1} = t_n.
```

In the algorithm, the value of  $\Theta_n$  is obtained from the small-kink angle (first-order) approximations to  $K_{I,II}^+$  in terms of  $K_{I,II}$  given in ? ]. Under this approximation, the angle  $\Theta_n$  is also the angle of Maximum Tensile Stress. Lastly, the expression for  $K_{In}^+$  is second order accurate in the mode mixity  $K_{II}/K_I$  to that of Cotterell and Rice.

In the numerical procedure above, only one of time and crack length is incremented in a given simulation step, which precludes direct calculation of the crack velocity from  $(a_{n+1} - a_n)/(t_{n+1} - t_n)$ . Instead, we estimate the crack velocity  $\dot{a}_n$  a posteriori in the following way. For any n with  $t_n < t_m$ , we let  $n_1 \le n$  be the smallest index such that  $t_{n_1} = t_n$ , and let  $n_2 \ge n$  be the smallest index such that  $t_{n_2} > t_n$ . Then, we estimate the velocity through the finite difference

$$\dot{a}_n = \frac{a_{n_2} - a_{n_1}}{t_{n_2} - t_{n_1}}.$$

Essentially, this procedure finds the two timesteps which bracket simulation step n, and uses those to estimate the velocity.

It becomes apparent at this point that there exist three discretization parameters: the mesh size h, the time stepping increment  $\Delta t$ , and lastly the arclength increment  $\Delta a$ . The numerical convergence of the crack path as h,  $\Delta t$ ,  $\Delta a \searrow 0$  has been verified through examples in [?]. Note that the sampling  $\{\xi_0, \ldots, \xi_m\}$  is conspicuously absent from the discretization parameters, as it should, since the time and crack parameterization is arbitrary. The choice of h,  $\Delta t$ , and  $\Delta a$  in our simulations was such that no variations in the crack path where observed with additional levels of refinement, as illustrated in §4.

Clearly, the value of the speed would not converge as the time step is refined for regions of supercritical propagation, in which the model would require an infinite speed. However, we provide the computed values anyhow later on in the manuscript.

#### 3.5. Choice of Discretization Parameters

The mesh utilized for the simulation was generated using a quad tree structure of mesh size  $h_{coarse} = L/48$ , where a portion of the domain with  $y \in (b/2, 3b/2)$  (the region in which the oscillations are expected to develop) was further refined to a mesh size  $h_{fine} = L/192$ . For all simulations the length of the domain was taken as L = 12 b.

Upon appearance of sharp features in the crack path, such as regions of high curvature or kinks, the mesh was adaptively refined as discussed in [?] to ensure that the conditions imposed by the algorithm that deforms the Universal Mesh on the background triangulations were satisfied. Furthermore, when the crack propagated into the portion of the domain with  $h > h_{fine}$ , the background mesh in such region was further refined.

Notably, because of the use of MFEM, the mesh did not need to be refined around the crack tip at each new crack geometry to observe numerical convergence. The only condition to refine the mesh was meshing sharp geometric features, and not improving the accuracy of the approximation. Figure 9 showcases a spatial discretization of the quenched plate at the end of one simulation, with locally refined regions near kinks. As mentioned, no refinement was performed around any of the partial cracks that lead to this final geometry, and the mesh shown here is the one deformed to mesh each one of the partial cracks away from the kinks as the crack grew.

The time stepping parameters and crack advancement parameters were chosen such that converged crack paths were observed, and these values were set to  $\Delta a = h_{fine}/8$  and  $\Delta t = 5 \Delta a/v$  (effectively the position of the cold front is advanced by  $5 \Delta a$ ). In all simulations, six-node quadratic triangles with curved edges

<sup>&</sup>lt;sup>1</sup>A caveat here is that kinks were automatically "regularized" by replacing the piecewise affine crack by a spline interpolation of the computed crack tips.

were adopted to build the MFEM spatial discretization. Lastly, in order to ensure a preferential direction of propagation, the initial notch was perturbed by 0.01 b in the positive y-direction.

## 3.6. Convergece of the Crack Path

To numerically verify the independence of the computed crack paths from the chosen values for the discretization parameters  $\Delta t$ , h and  $\Delta a$  in §3.5, we recomputed a subset of all the calculations we performed after halving the values of the three discretization parameters. Results for two such cases are shown in Figs. 10 and 11, which show that in fact the difference between the paths computed with the two sets of parameters is negligible. Even though at this time there is no proof that the crack paths computed by the numerical method do in fact converge, these results strongly suggest that this is the case.

## 4. Results

Experimental results [? ? ? ? ? ], as well as dimensional analysis [? ], show that primarily two non-dimensional parameters control the behavior of crack propagation. These parameters are the Peclet Number defined as

$$P = \frac{bv}{D},\tag{10}$$

and the non-dimensional toughness (and its reciprocal) defined as

$$\hat{K}_C = \frac{K_C}{\alpha E \Delta \mathsf{T} \sqrt{b}} = \hat{R}^{-1}.$$
 (11)

Here E is Young's modulus, given by

$$E = \frac{\mu(3\lambda + 2\mu)}{\lambda + \mu}.$$

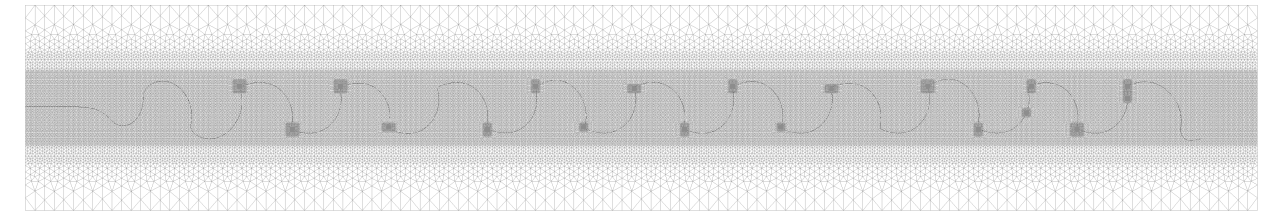
In what follows we explore the regimes of crack propagation by varying these control parameters. We start with a brief discussion in §4.1 of the evolution of a crack through a kink as observed in the simulations herein. We highlight how the stress intensity factors and the mode mixity vary with respect to the parameterization. In §4.2, through a dense and vast exploration of phase space, we contrast the accuracy of the computed results with analytical ones, particularly we compare the computed thresholds from stationary crack to straight crack propagation as well as from straight to oscillatory crack propagation with analytical ones. In §4.2 we highlight the different geometrical characteristics of the computed crack paths and contrast them with the ones observed in experiments. For those cracks that oscillate, in §4.4.2 we explore their frequency content as a function of P and  $\hat{K}_C$ . Following, in §4.5, we highlight the peculiar feature of supercritical crack propagation followed by sudden crack arrest. Lastly we discuss in §4.5.2 the observed sharped initial change of direction of the crack followed by potential crack branching. Throughout we re-connect computations with analytical as well as experimental results available in the literature.

To give the reader a sense of scale, cracks are plotted on background grids of dimension  $0.25 b \times 0.25 b$ , unless otherwise noted.

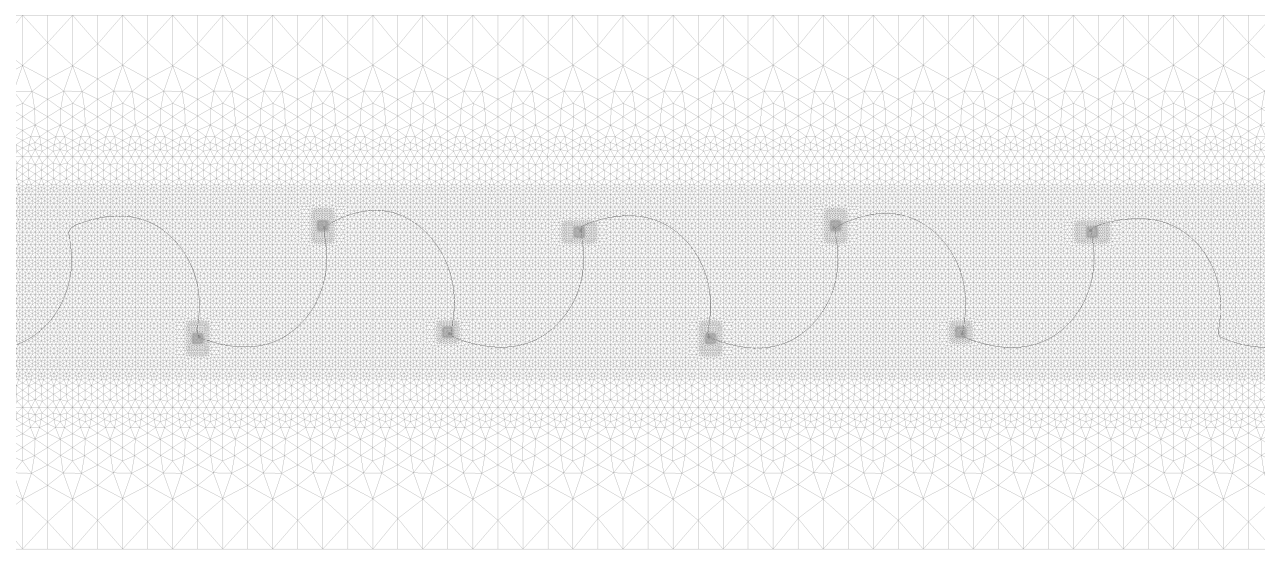
## 4.1. Introductory Discussion: Crack Evolution Through a Kink

The key feature of the crack evolution model presented in Problem 2.3 is its ability to describe evolutions with kinking (where the crack tangent rapidly changes direction) and with bursts of supercritical growth (where  $K_I^+ > K_C$ , and the crack propagates a finite distance in an infinitesimal time). Here, we briefly showcase the evolution of the crack through a kink. As will be discussed in later sections, depending on the values of the non-dimensional parameters, the crack may experience both kinking and supercritical growth, with the two often appearing hand-in-hand.

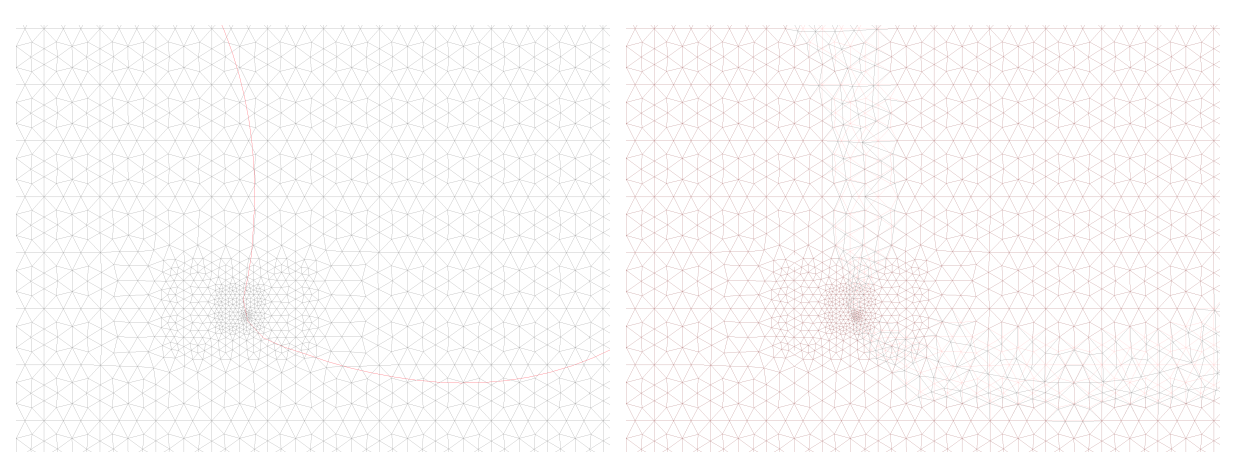
In Fig. 12, we show the evolution of a crack which experiences both kinking and supercritical growth for the case with P = 3.0 and  $\hat{R} = 18.0$ . Because we do not explicitly specify a parameterization for the evolution, we choose to parameterize using the simulation step number. We recall that, in our numerical evolution scheme, at each simulation step we either advance the loading by moving the cold front or we advance the crack. Hence, plotting the crack length versus the position of the cold front yields a curve which resembles a staircase, as shown in Fig. 12.



(a) A sample background mesh used as a Universal Mesh.



(b) Zoom in of the background mesh highlighting the various regions of refinement.



(c) Detail around a sharp feature of the background mesh. (d) Detail around a sharp feature of the conformed mesh (in gray) alongside the background mesh (beneath in red).

Figure 9: A sample Universal Mesh ( $P=3.0,\,\hat{R}=18.0$ ).

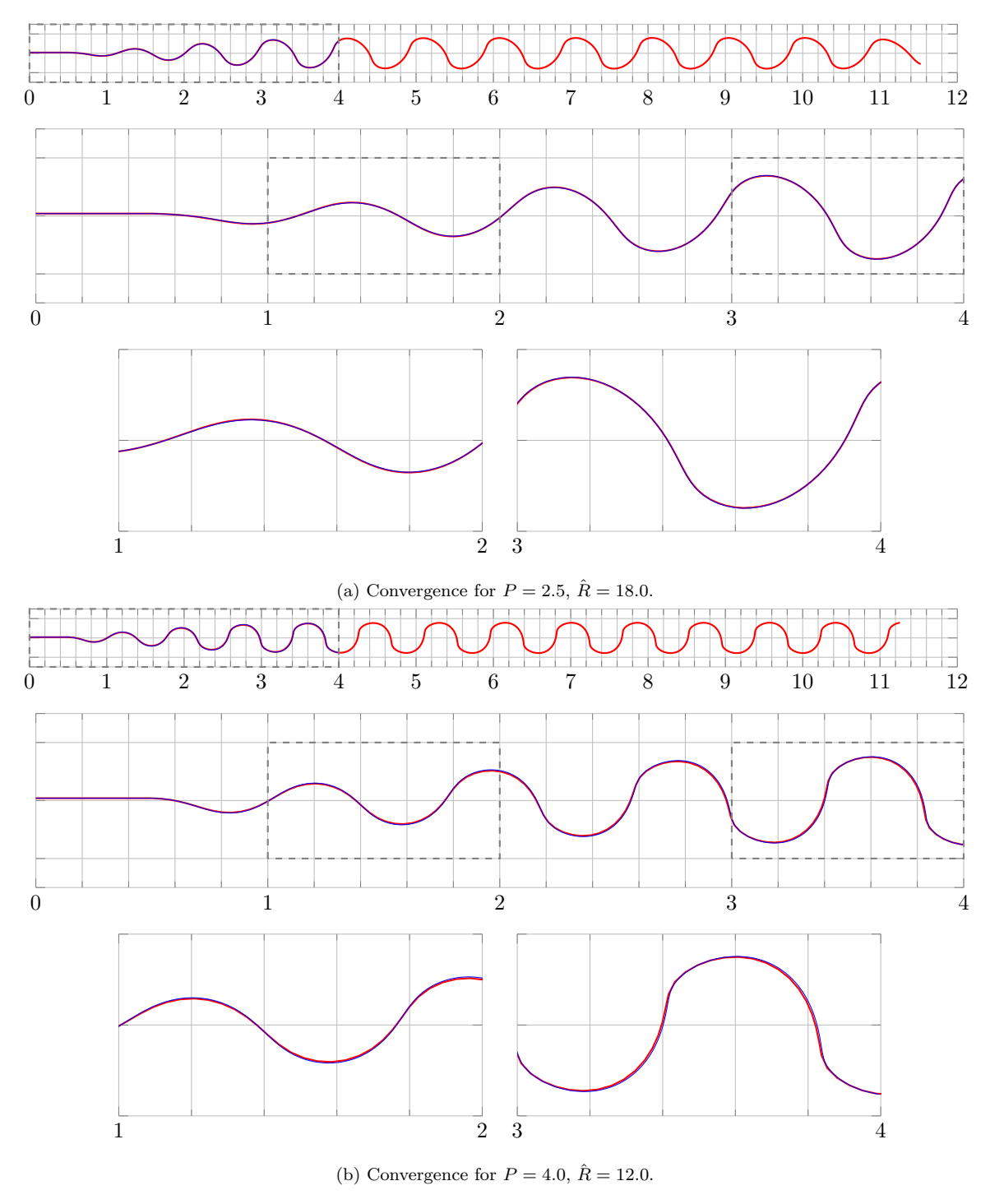
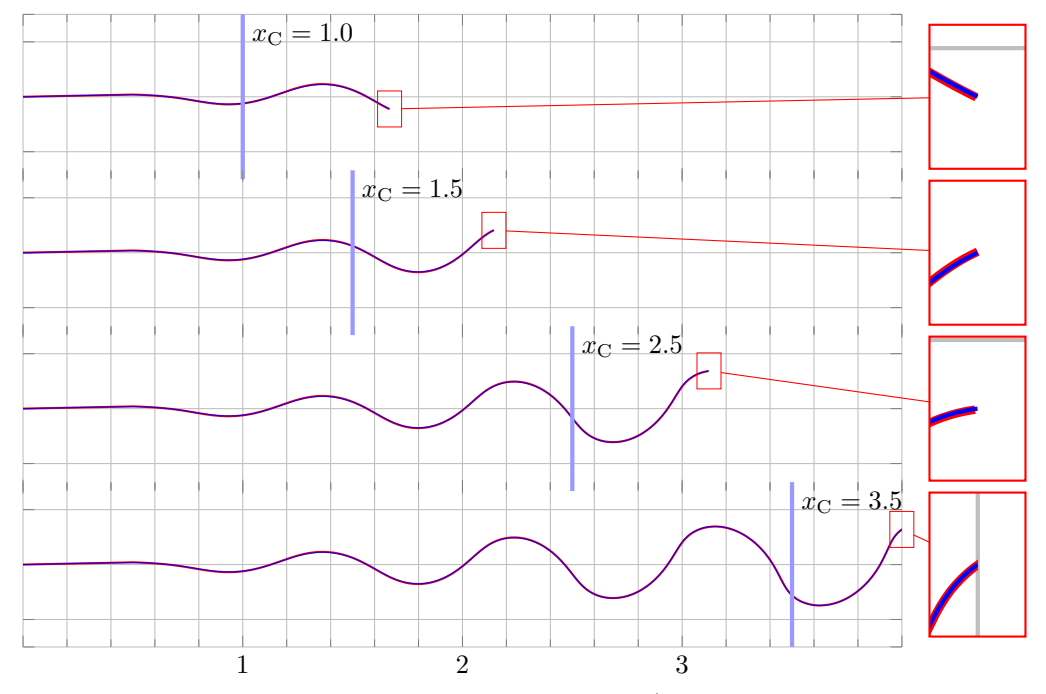
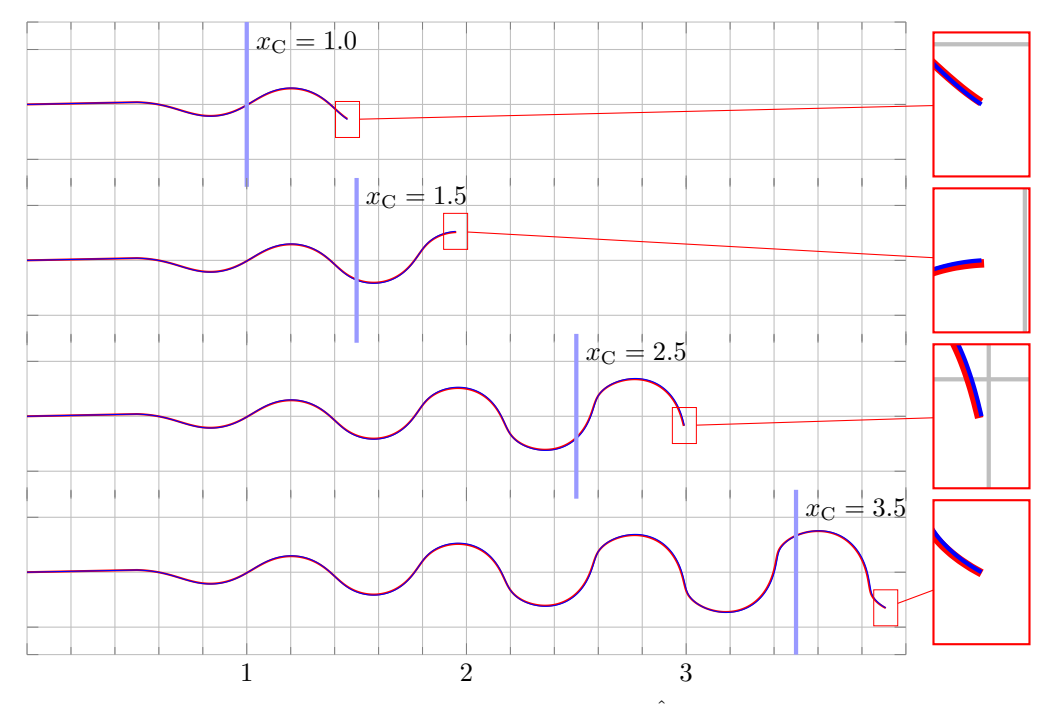


Figure 10: Convergence of the computed crack paths. The red curves show the computed crack paths with the discretization parameters described in §3.5 while the blue curves show the computed crack paths when the same parameters are halved. Negligible differences arises in the computed crack paths suggesting that the parameters of §3.5 are appropriate for the convergent computation of the crack paths.



(a) Time convergence for P=2.5 and  $\hat{R}=18.0$ .



(b) Time convergence for P=4.0 and  $\hat{R}=12.0$ .

Figure 11: Time convergence of the computed crack paths. Time is here indicated by the position of the cold front, given that the immersion velocity is held fixed. Only minor differences arise in the computed position of the crack tip for the discretization parameters of §3.5 (here shown in red) and the one with the discretization parameters halved (blue curves).

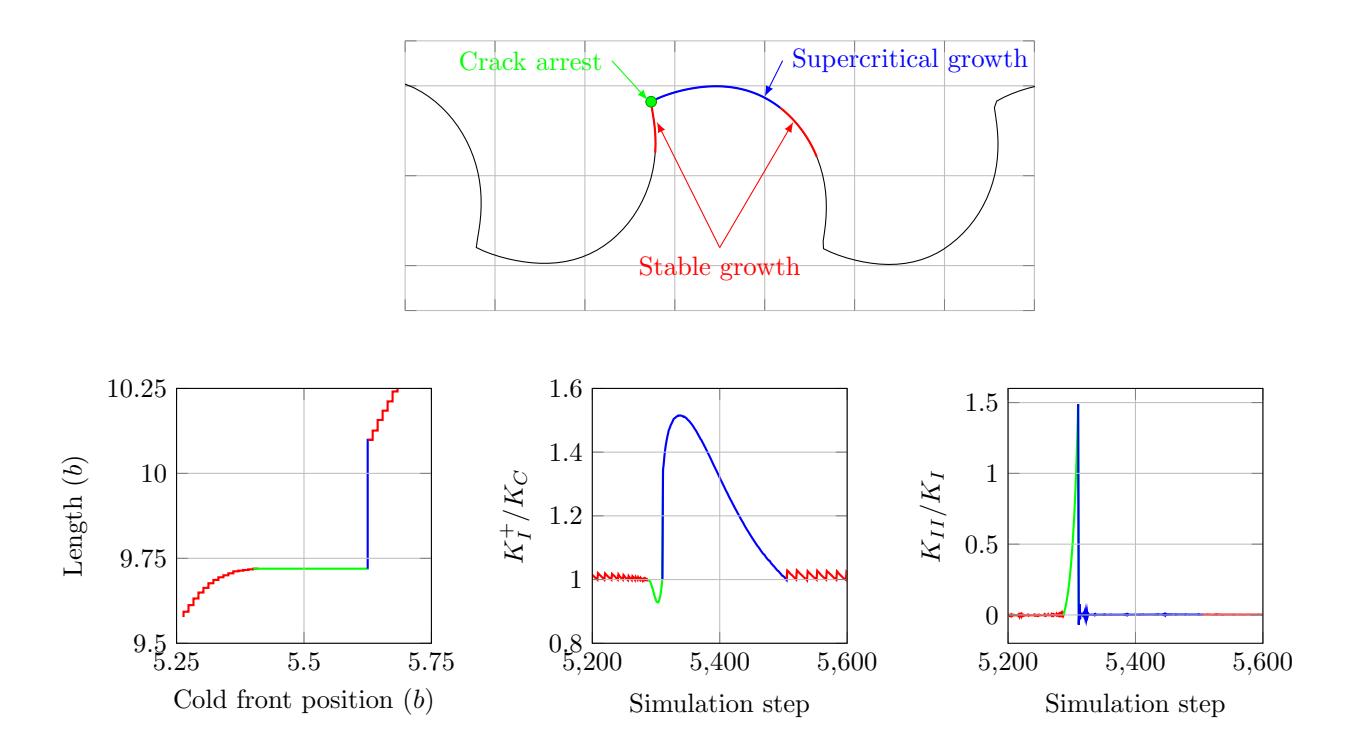


Figure 12: Evolution of a crack through a kink with non-dimensional parameters  $(P, \hat{R}) = (3.0, 18.0)$ . (Top) Close-up of the crack path, highlighting the region studied. The grid has dimensions  $0.25 \, b \times 0.25 \, b$ . (Bottom, from left to right) The length of the crack versus the position of the cold front, the stress intensity factor  $K_I^+$  versus the simulation step, and the mode mixity versus the simulation step.

The growth of the crack through a kink can be broken down into stages, which are color-coded in Fig. 12. The crack begins propagating stably with  $K_I^+ = K_C$  (depicted in red). As the crack turns away from the direction of immersion, it arrests, with  $K_I^+$  dropping below  $K_C$  (shown in green). The cold front continues to advance, and the mode mixity at the crack tip changes with mode II increasing. The increase in mode II raises the value of  $K_I^+$  back up to  $K_C$ , and the crack kinks. Following the kink (in blue),  $K_I^+$  grows rapidly, while the mode II stress intensity factor drops almost instantaneously to zero. The crack has become supercritical, and it continues to grow along a path of  $K_{II} = 0$  before returning back to critical growth.

## 4.2. Phase Space of the Problem

The two non-dimensional parameters  $\hat{K}_C$  (or its reciprocal  $\hat{R}$ ) and P define a two-dimensional phase space for this problem. The following sections explore features of the cracks predicted by the model. The model gives rise to four qualitatively different crack evolutions:<sup>2</sup>

• No propagation: as the plate is immersed no crack advancement is observed.



• Straight propagation: the crack propagates along the bisector of the plate.

<sup>&</sup>lt;sup>2</sup>The four sample cracks correspond to  $(P, \hat{R}) = (3.0, 3.0), (3.0, 10.0), (3.0, 17.0), (3.5, 18.5)$  for no propagation, straight propagation, oscillatory propagation, and snap back, respectively.



 Oscillatory propagation: the crack propagates along a wavy crack path. The path may not be smooth, with kinks appearing.



• Snap back: the crack turns backward and is suddenly arrested. Beyond this point, the crack may turn back to continue propagating, and may even branch (as seen in experiments [?] and as evaluated in a heuristic manner in §4.5.1).



In order to understand the formation and evolution of the crack patterns, several crack paths were computed on a regular grid in phase space ( $\hat{R}$  vs. P). Figure 13 illustrates the results, in which each crack is classified into one of the four categories defined above. After classifications, distinct regions of the phase space yielded different crack responses and clear thresholds emerged between no propagation and straight propagation (which will be referred to as the *propagation threshold*), as well as between straight propagation and oscillatory propagation (which will be referred to as the *oscillatory threshold*). Additionally a new threshold appears between oscillatory propagation and snap back (which will be referred to as the *snap back threshold*). This last threshold seems to be new to the literature.

In an effort to verify the results, the computed response in phase space, shown as markers in Fig. 13, was compared against threshold lines obtained analytically through perturbation analysis [?]. The blue line in Fig. 13 highlights the analytical propagation threshold, while the red line highlights the analytical oscillatory threshold. Both computed and analytical thresholds essentially coincide, as they should. This is because in both cases the same problem is being solved, namely Problems 2.1, 2.2, and 2.3, and the computational results are converged (c.f. §3.6). In fact, the close agreement between both thresholds further enhances the confidence in the convergence of the numerical results beyond the earlier tests showcased in Figs. 10 and 11.

## 4.3. Straight Crack Propagation

As previously discussed, in order to trigger the instability, as well as to control the preferential direction of the first oscillation, the initial notch was shifted by  $0.01\,b$  in the positive-y direction. This implies that in the case of "straight crack" propagation, the crack would be expected to advance towards the centerline of the plate, and once it reaches the centerline, to continue propagating along it.

Interestingly, as the oscillatory threshold is approached, the crack path resembles the amplitude response of a harmonic oscillator where, depending on the distance to the threshold in phase space, it exhibits an over-, critically-, or under-damped response. More specifically, the crack path either takes a really long time to return to the centerline, it returns to centerline line rather rapidly, or it oscillates with decaying amplitude about the centerline until it propagates steadily along it. Figure 14 illustrates this behavior, where for some parameters the crack path returns to the centerline with varying speed (over- or critically damped), while for many other cases the crack path oscillates with a decaying amplitude until the centerline is reached. Past the threshold, the crack path resembles that amplitude reponse of an undamped oscillator, and the properties of these types of cracks is discussed in the next section.

### 4.4. Oscillatory Crack Propagation

Beyond the straight crack propagation regime, cracks begin to propagate along wavy patterns. These oscillatory cracks possess several rich features in terms of frequency content, amplitude variations, morphology, and speed of propagation. In what follows we discuss all of these features and highlight regions of phase space where they occur.

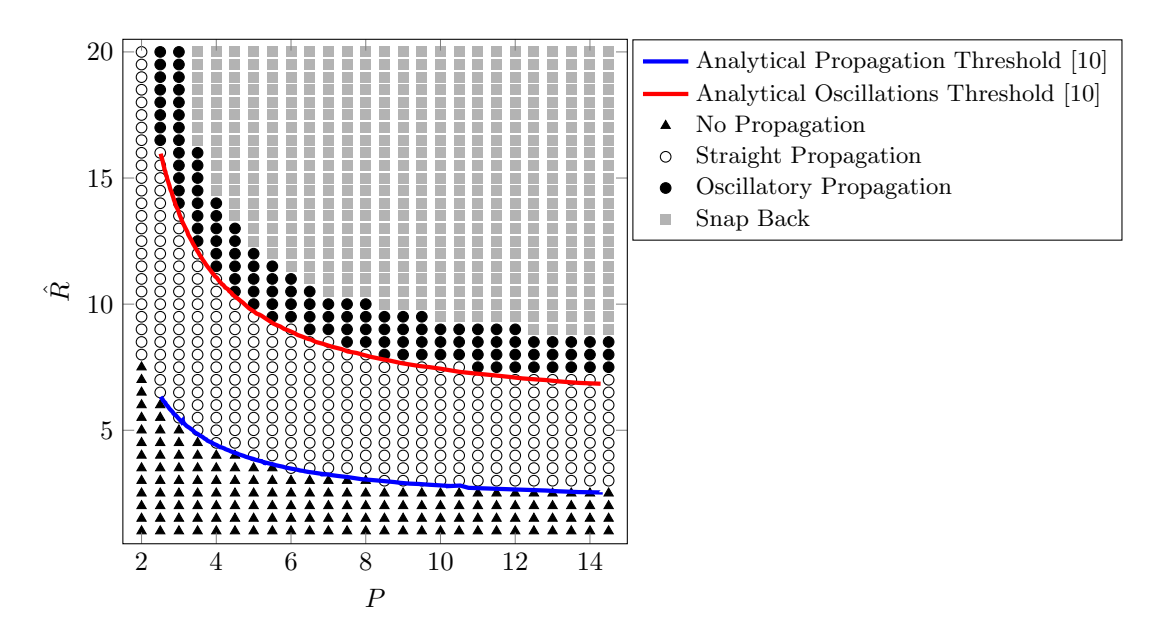


Figure 13: A computed region of the phase space of crack evolutions. Each circle, triangle, or square indicates that the crack evolution for the corresponding values of  $(P, \hat{R})$  has been computed, and its evolution classified according to the categories in §4.2. Also shown are comparisons with the analytically computed thresholds in [?]. The close agreement further validates the accuracy of the computed results.

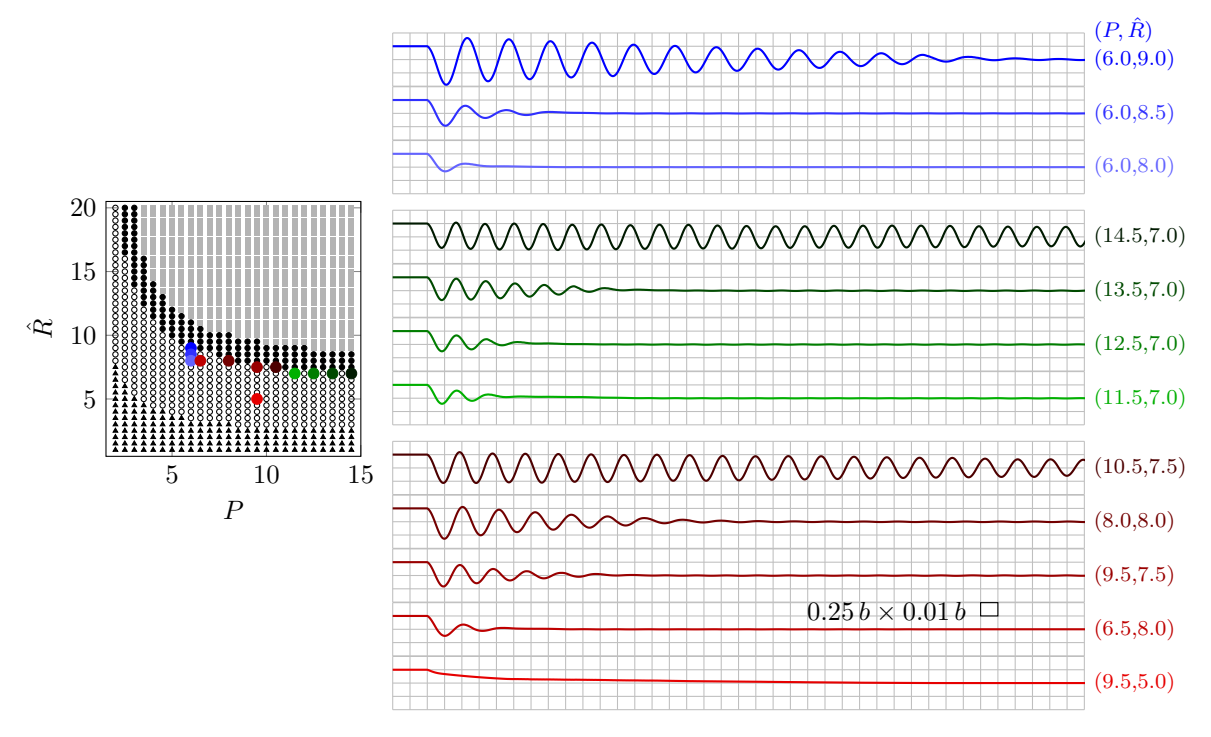


Figure 14: Sample crack paths in the neighborhood of the oscillatory threshold in phase space, showing the over-, critically, and under-damped harmonic-oscillator-like response of the crack path. The color of the curve indicates the location in the phase space diagram on the left.

## 4.4.1. Morphology of Oscillations

A very interesting aspect of the oscillatory cracks is that not all oscillations look alike. Namely, depending on the values of P and  $\hat{R}$ , the morphology of oscillations varies drastically ranging from smooth wave like oscillations to sharply kinked patterns.

Figure 15 showcases four representative crack path patterns observed in the simulations. These four sample crack paths were chosen solely based on the pronounced nature of the morphology in discussion; many other crack paths in phase space could have equivalently been used as representatives of these morphological features.

The crack path corresponding to  $(P = 2.5, \hat{R} = 18.5)$  (at the top of Fig. 15(a)) showcases wave-like sinusoidal oscillations. The characteristic of these cracks is their smooth nature alongside a reasonably constant speed of propagation on the order of the speed of immersion.

The crack path corresponding to  $(P = 5.0, \hat{R} = 10.5)$  (second from the top in Fig. 15(a)) illustrates semi-circle oscillations as observed in [? ? ]. Similar to wave-like cracks, the speed of propagation is on the order of the speed of immersion; the distance between the cold front and the crack tip does not vary considerably.

The crack path corresponding to  $(P=3.0, \hat{R}=18.0)$  (third from the top in Fig. 15(a)) captures the behavior described in [?], in which they noticed the crack growing almost entirely in the y-direction, only to continue growing in the x-direction after forming a kink. In the language introduced in [?, Fig. 12d], this morphology is label "crack cusping," and the discontinuity in the tangent to the crack path is labeled a "cusp." Interestingly, as the crack approaches the location of kinking, it suddenly slows down considerably, allowing for the cold front to get closer, and following a period of arrest it propagates again rather quickly (approximately twice as fast as the cold front).

Lastly we observed an additional behavior, exemplified by the crack path computed for  $(P = 6.0, \hat{R} = 10.0)$  (in light red in Fig. 15(a)), where the crack grows entirely in the y-direction and shortly thereafter propagates along a straight line, almost as a flattened sinusoidal curve, only to continue to undertake undulations again. Similar to cusping cracks, this class of cracks undergo considerable changes in propagation speed and the cold front and the crack tip seem to be in a regimen of catch up. Namely, the crack tip advances rapidly until it stops to let the cold front get closer only to rapidly move away from it again following a kink.

### 4.4.2. Frequency Content and Amplitudes

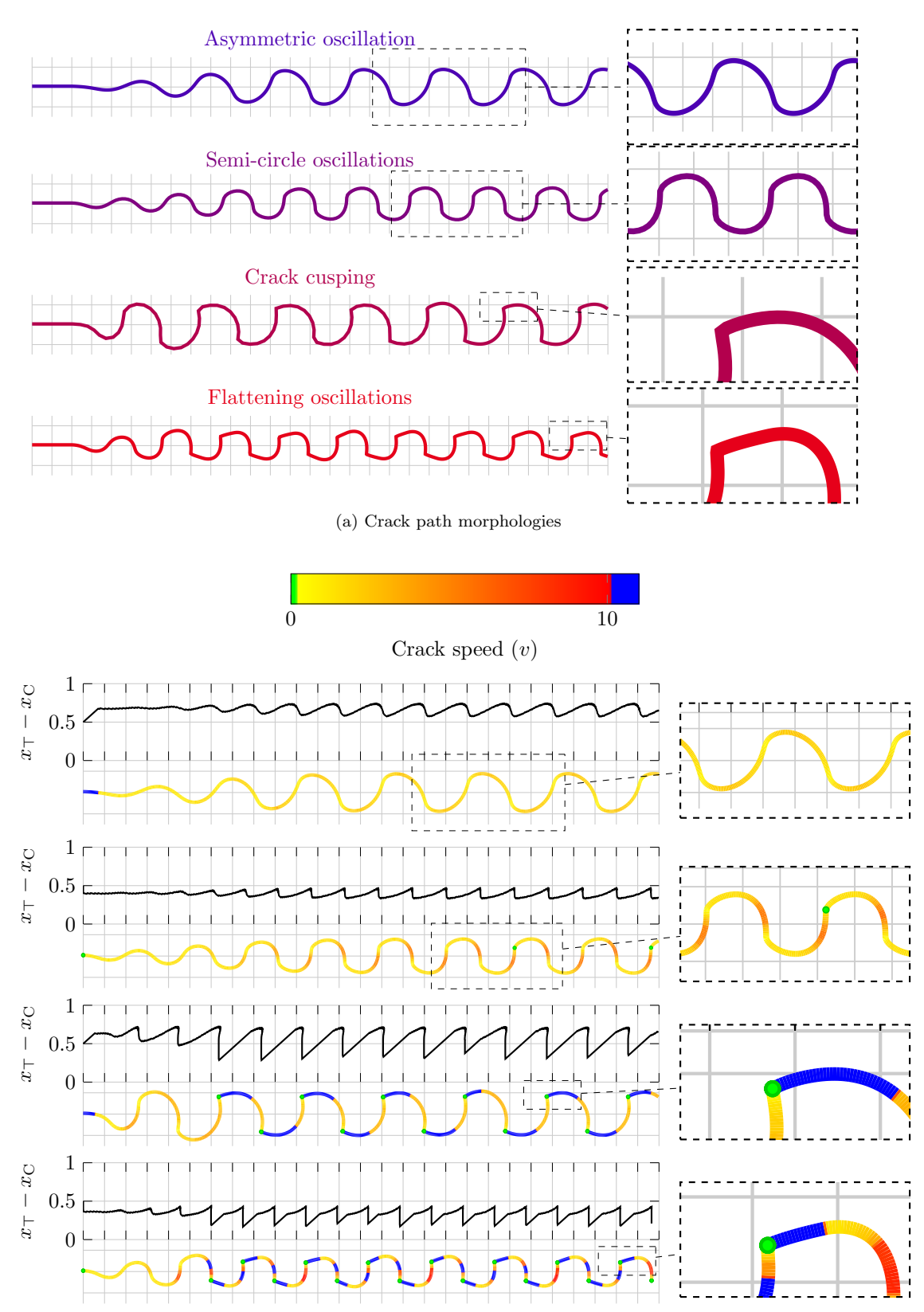
Besides the geometrical features of each crack, it is rather interesting to note that both the amplitudes and the frequency content of the oscillations vary considerably in phase space. Figure 16(a) showcases the evolution of the oscillations along a vertical direction (i.e. with fixed P) in phase space. The shown crack paths correspond to P=3.0 and  $\hat{R}=12.5,13,\ldots,18$ . It is evident that the amplitude grows as the value of  $\hat{R}$  moves away from the threshold and, upon a closer look, multiple periods of oscillations develop, as was noticed in [?].

We further investigated the spectral behavior of these oscillations. The vertical crack tip position is not a function of the horizontal crack tip position (see the inset for P=3.0 and  $\hat{R}=18.0$  in Fig. 15(b)), and hence we could not analyze  $y_{\top}(x_{\top})$ . Instead, we performed a Fast Fourier Transform of the vertical crack tip position as a function of the position of the cold front (i.e.  $y_{\top}(x_C)$ , shown in Fig. 16(b)), which was sampled at 1024 uniformly-spaced points.

The computed frequency spectra are shown in Fig. 17. They all contain a predominant or primitive frequency, and they display the appearance of additional odd harmonics of this frequency. This is in qualitative agreement with the spectra in Fig. 13(b) and (c) of ? ]<sup>3</sup>. For the value  $\hat{R} = 17.5$ , we note the appearance of a triple period. This triple period can further be observed in Fig. 16(b), where small bumps appear on every third oscillation. We compare the spectrum for this case with Fig. 13(d) in [? ]. In [? ? ], the authors observed a double period, which we found for other values of P in phase space, namely  $(P, \hat{R}) = (4.5, 12.0)$ , (5.0, 11.0), (6.0, 9.5), (7.0, 9.0), and (9.0, 8.0).

Additionally, we show in Fig. 18 the variation in phase space of the amplitudes (defined as the maximum offset of the crack tip position from the centerline) and the wave length (taken as the primitive period for oscillatory cracks), and two interesting trends appear. First, for a fixed Peclet number P, the amplitudes

<sup>&</sup>lt;sup>3</sup>The agreement is necessary qualitative because the cited reference does not provide data to compute  $(P, \hat{R})$  for these results.



(b) Crack paths speed. The speed of the crack is plotted in units of the speed of immersion v, namely the contour shows  $\dot{a}/v$ . Values of  $\dot{a}/v > 10$  are depicted in blue.

Figure 15: Crack path morphologies and velocities for oscillatory cracks. From top to bottom the cracks correspond to  $(P, \hat{R}) = (2.5, 18.5), (5.0, 10.5), (3.0, 18.0), (6.0, 10.0)$ . The background grid size is  $0.25 \, b \times 0.25 \, b$ .

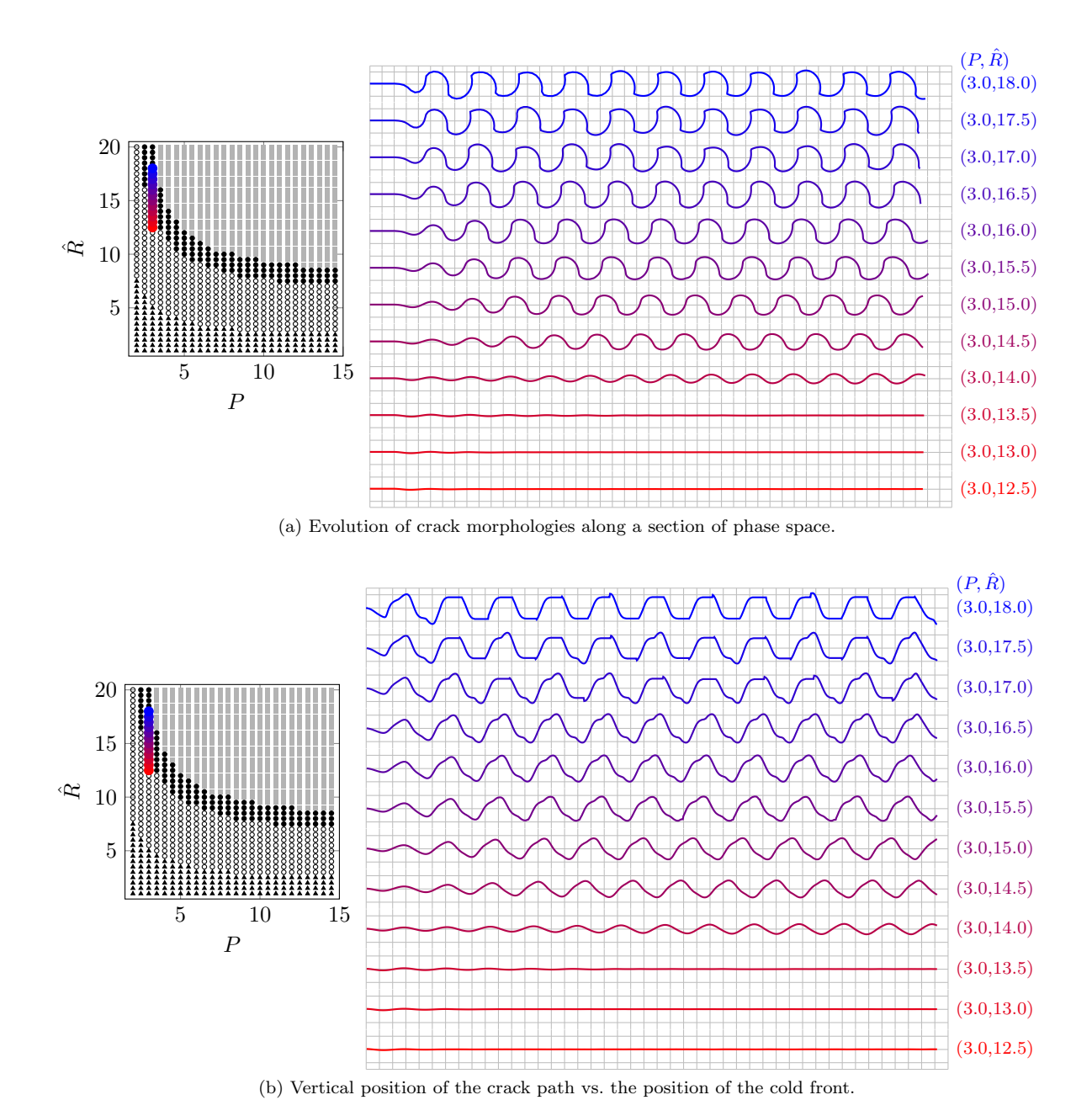


Figure 16: Development of crack path oscillations in phase space (top) and vertical position of the crack path vs. the position of the cold front, which effectively represents time (bottom). In both cases, the crack paths were computed for P=3.0 and for  $\hat{R}$  starting at 12.5 (lowermost crack path) and then increasing in 0.5 increments up to  $\hat{R}=18.0$ . The curves in (b) were used to compute the power spectra shown in Fig. 17. The color of the curves indicate their location in the phase space diagram on the left. Each square in the background grid has size  $0.25\,b\times0.25\,b$ .

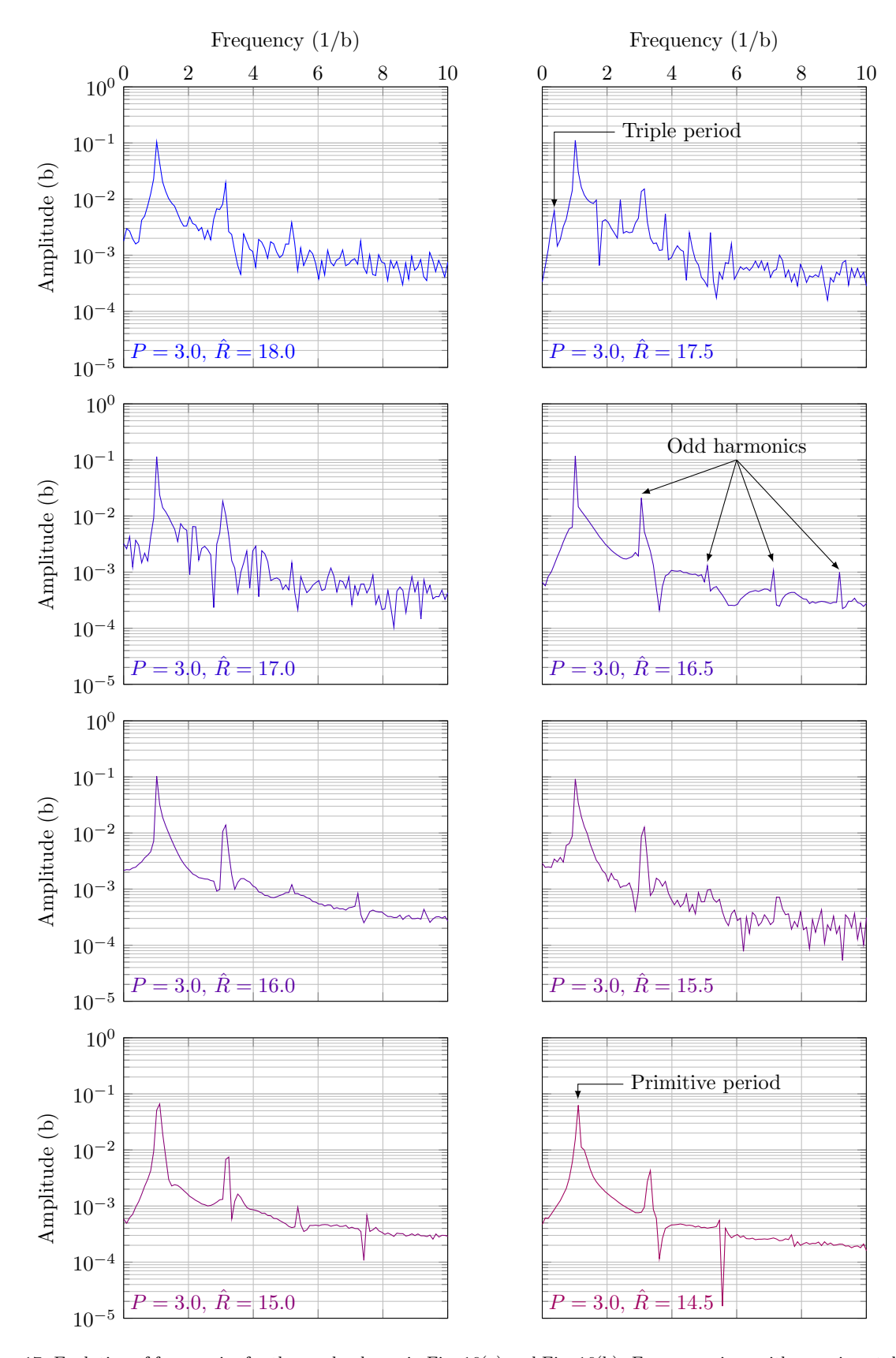


Figure 17: Evolution of frequencies for the cracks shown in Fig. 16(a) and Fig. 16(b). For comparison with experimental results see [? , Fig. 13].

grow as the non-dimensional toughness decreases (or  $\hat{R}$  increases), transitioning continuously through the oscillatory threshold. Beyond the oscillatory threshold, the amplitude appears to grow like  $\hat{R}^{1/2}$ , as noted in both [?, Fig. 5(a)] and [?, Fig. 4]. Second, the wave length of the oscillatory cracks increase as the Peclet number is reduced. This behavior is again qualitatively similar to that observed in [?, Fig. 10].

Lastly, apart from the triple period of oscillations in Fig. 17, there exist periodic recurrences of the appearance of morphological features (i.e., flattening oscillations, cusping, etc.), as illustrated in Fig. 19. This was also observed experimentally in [?, Fig. 12 (particularly Fig.12(d))].

### 4.5. Beyond Oscillatory Propagation

Further away from the threshold between straight and oscillatory crack propagation, it becomes rather challenging to derive analytical results, and it is in this particular region of phase space that numerical methods, as well as experiments, are instrumental in providing insight on the system's behavior. In what follows we describe the response in this particular region of phase space, in which supercritical crack propagation, crack kinking, and crack branching are all expected.

### 4.5.1. Supercritical Crack Propagation and Crack Kinking

In addition to the aforementioned post mortem geometric features of the crack paths (i.e., frequency content, amplitudes, etc.), it is interesting to investigate the transient crack propagation behavior. As it was highlighted in [?], the cracks were observed to undertake short periods of sudden, supercritical crack propagation, which they labeled as "unstable" crack propagation.

These short periods of supercritical propagation were similarly identified in our computation, whereby after a short arrest, the crack was observed to continue to propagate. Fig. 20 illustrates the short periods of supercritical crack propagation by highlighting in yellow markers the portion of the cracks where the propagation was supercritical (namely  $K_I > K_C$ ).

The periods of supercritical propagation occur after kinking takes place. Additionally, by exploring the crack tip velocity, as evident in Fig. 15 and Fig. 20, we see that the crack propagates rapidly almost entirely in the y-direction only to arrest, and afterwards, following a kink, it propagates in a supercritical state.

### 4.5.2. Snap Back, Snap Forward, and Branching

Lastly, crack path behaviors further away for the oscillatory threshold are explored. In Fig. 21, we show the evolution of the computed crack path as we move away from the threshold between straight and oscillatory crack propagation. First we observe that the crack sharply turns back, and for smaller values of the Peclet number the crack arrests. As the Peclet number is further increased, the crack is able to turn around and continue propagating. Similar behavior was observed in [?, cf. Fig. 15(a) and Fig. 16(j)], where the sharp turn was further accompanied by crack branching.

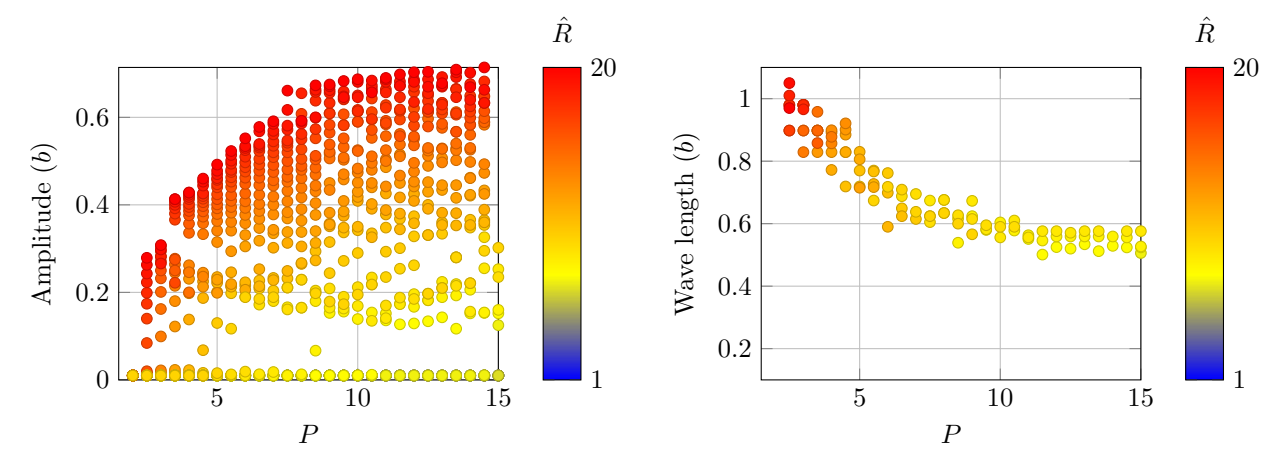
The observation that crack branching may occur in certain regions of the phase space served as a motivation to formulate a heuristic or empirical model to establish whether or not crack branching may occur, even though in the model considered here dynamic effects are not accounted for. To this end, the results in ? ] were adopted as a way to estimate the speed of the crack as a function of the overstress  $K_I - K_C$ , even though the cracks considered here do not propagate at a constant speed or a straight path. These state that

$$\frac{\dot{a}}{c_R} \approx H(K_I - K_C) \left( 1 - \frac{K_C^2}{K_I^2} \right),\tag{12}$$

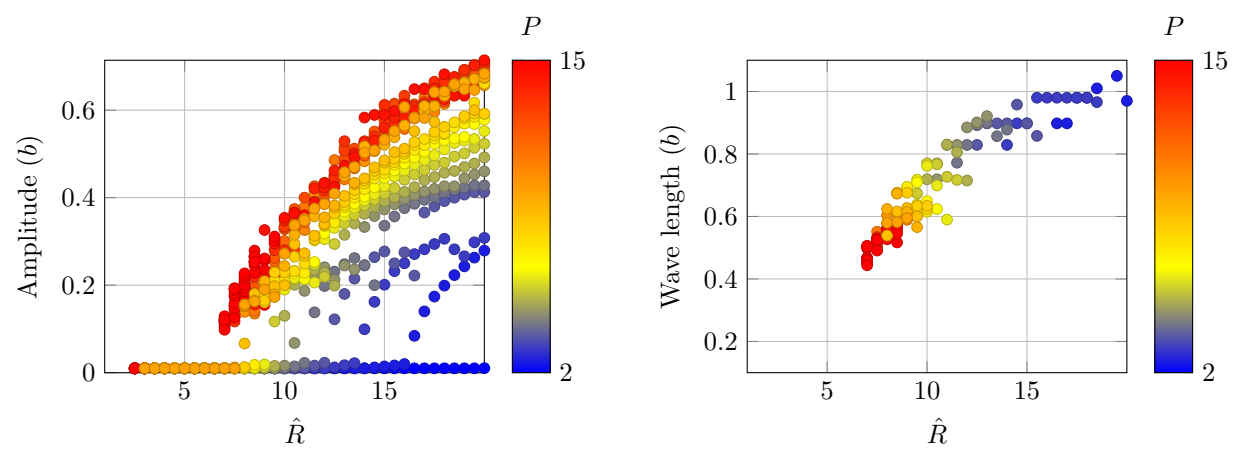
where  $\dot{a}$  is the speed of the crack,  $c_R$  is the Rayleigh wave speed of the material, and H(x) is the Heaviside function. The crack is deemed to bifurcate if it satisfies Yoffe's criterion [?], which predicts the occurrence of two symmetric peaks of normal stress on inclined planes at speeds  $\dot{a}$  that are around 66% of the Rayleigh-wave speed<sup>4</sup>. Combining these two results suggest that branching occurs if, at any stage of crack growth,

$$\frac{K_I^2}{K_C^2} \ge 2.9. (13)$$

<sup>&</sup>lt;sup>4</sup>In [? ?], the onset of symmetric peaks of normal stress occurs at approximately 60% of the shear wave speed. For  $\nu \approx 0.23$ , the Rayleigh wave speed is roughly 92% of the shear wave speed, giving the above result.



(a) Variation of the amplitudes (left, cf. Fig. 5(b) in [? ]) and the wave length (right, cf. Fig. 10 in [? ]) as a function of the Peclet number



(b) Variation of the amplitudes (left, cf. Fig. 5(a) in [?]) and the wave length (right) as a function of the reciprocal toughness

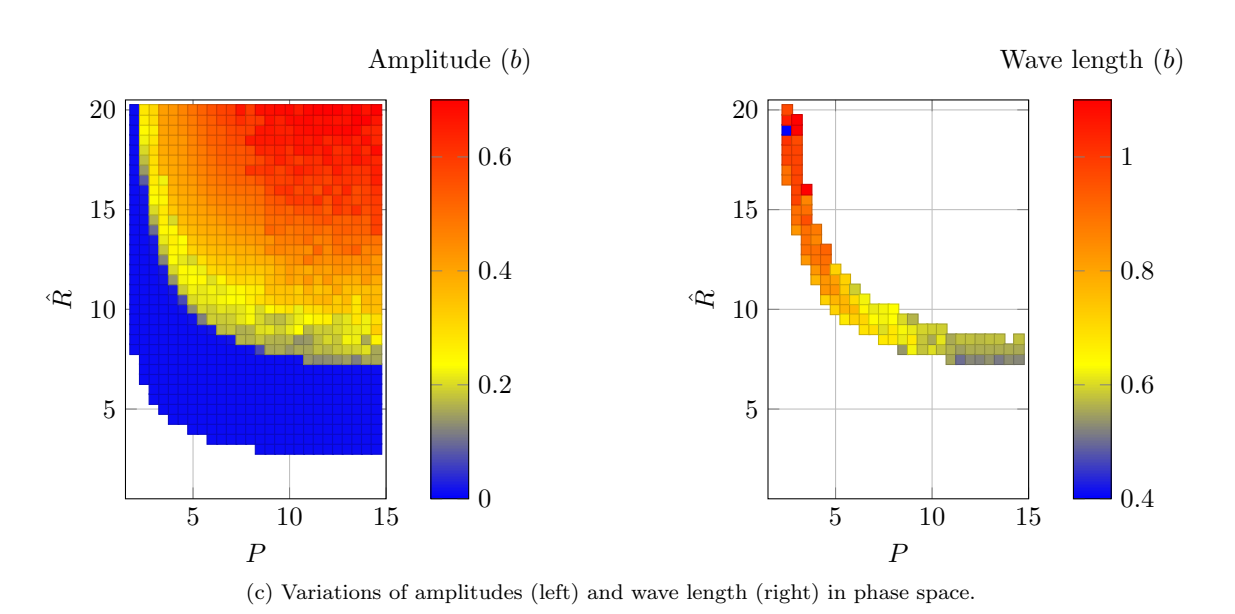


Figure 18: The variation of amplitudes (left column) and wave length (right column) versus  $\hat{R}$ , and in phase space. The amplitude is defined as the maximum offset of the crack tip position from the centerline. The wave length is taken for the primitive frequency, and only exists for oscillatory propagation.

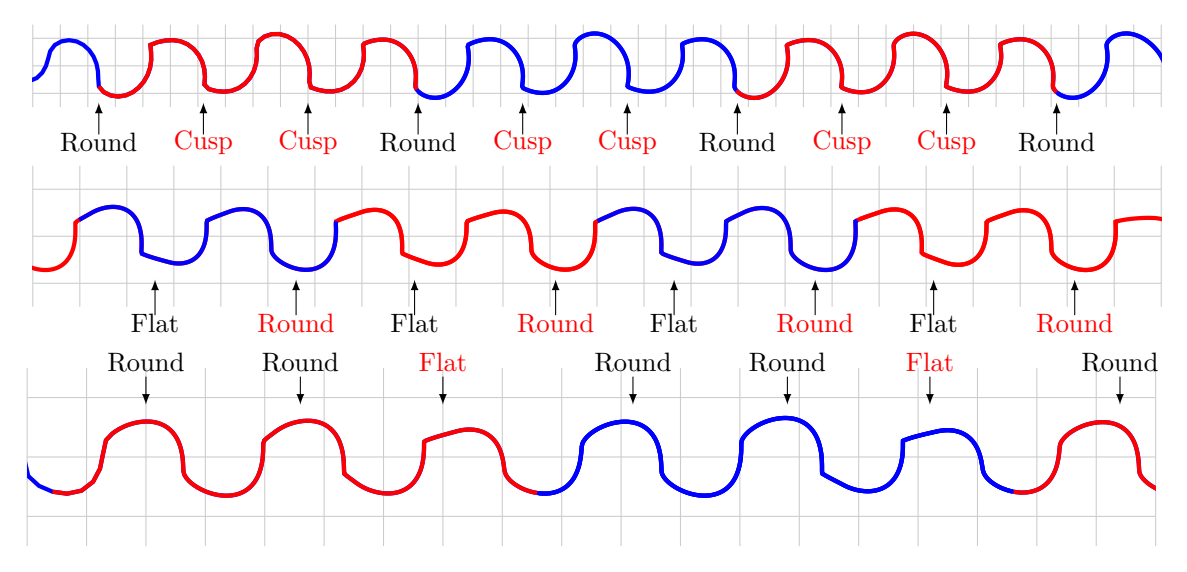


Figure 19: Examples of the periodic recurrence of crack path morphological features. Additionally to the appearance of a second period, there exists a an alternating recurrence of morphological features such as crack cusping, flat-top, and wave and each square in the background grids is of size  $0.25 b \times 0.25 b$ . The above cracks correspond to, starting from the top,  $(P, \hat{R}) = (3.0, 17.5), (7.0, 9.0), (7.5, 8.5)$ .

Categorizing cracks according to (13) gives rise to the appearance of a new threshold in phase space between snap back and possible branching. The computed cracks in phase space which according to the above empirical approach may be branching are highlighted with squares with a red border in Fig. 22. We note the appearance of three outlier cases. In these cases, (13) is true for no more than 1% of simulation steps (in comparison, for the other cases (13) is true at 5% or more simulation steps). In the same figure, two new thresholds in phase space were drawn. The first one is between oscillatory crack propagation and snap back ( $\hat{R}_{\text{Snap}}(P)$ ), and the second one is the threshold that indicates the transition to crack branching ( $\hat{R}_{\text{Branch}}(P)$ ). These two curves are the result of polynomial fits through selected representative points. The coefficients of the posynomials, as well as their powers, are provided in Appendix B in Table B.2.

In an effort to validate such a heuristic approach to predicting branching, the computed thresholds were compared with the one experimentally observed by ? ]. The comparison is also depicted in Fig. 22, which shows that the heuristic approach appears to be a conservative estimate for branching.

## 5. Summary

We proposed an extension of the model in [? ] to cracks that kink in two dimensions, and built a computational framework to compute the prediction of such model on cracks propagating in rectangular plates subjected to thermal gradients. The results of the mathematical model compared favorably against experimental and analytical results, and were verified to be both spatially and temporally converged. With these tools at hand, we recovered several propagation regimes that have been experimentally observed, and some of them not analytically obtained (snap back, and potential for branching). Additionally, we identified candidate thresholds in phase space that correspond to both snap-back and to branching, and provided approximate curve fits for them. The branching threshold was identified through a heuristic model based on the relationship between the crack speed and the overstress in a simpler dynamic fracture problem [?], and Yoffe's criterion [?] for crack branching. For such a coarse model, the agreement with experiments was deemed qualitatively good. Additionally, we identified different oscillatory crack path morphologies (wave-like, semi-circular, flattened oscillations, and kinked oscillations), and the speed at which the crack transverses them, including instances of crack arrest and supercritical propagation. We were also able to capture the frequency content observed in experiments of the oscillatory cracks, including the appearance of mophological features with periods that double or triple the fundamental one; the latter has not yet been experimentally reported.

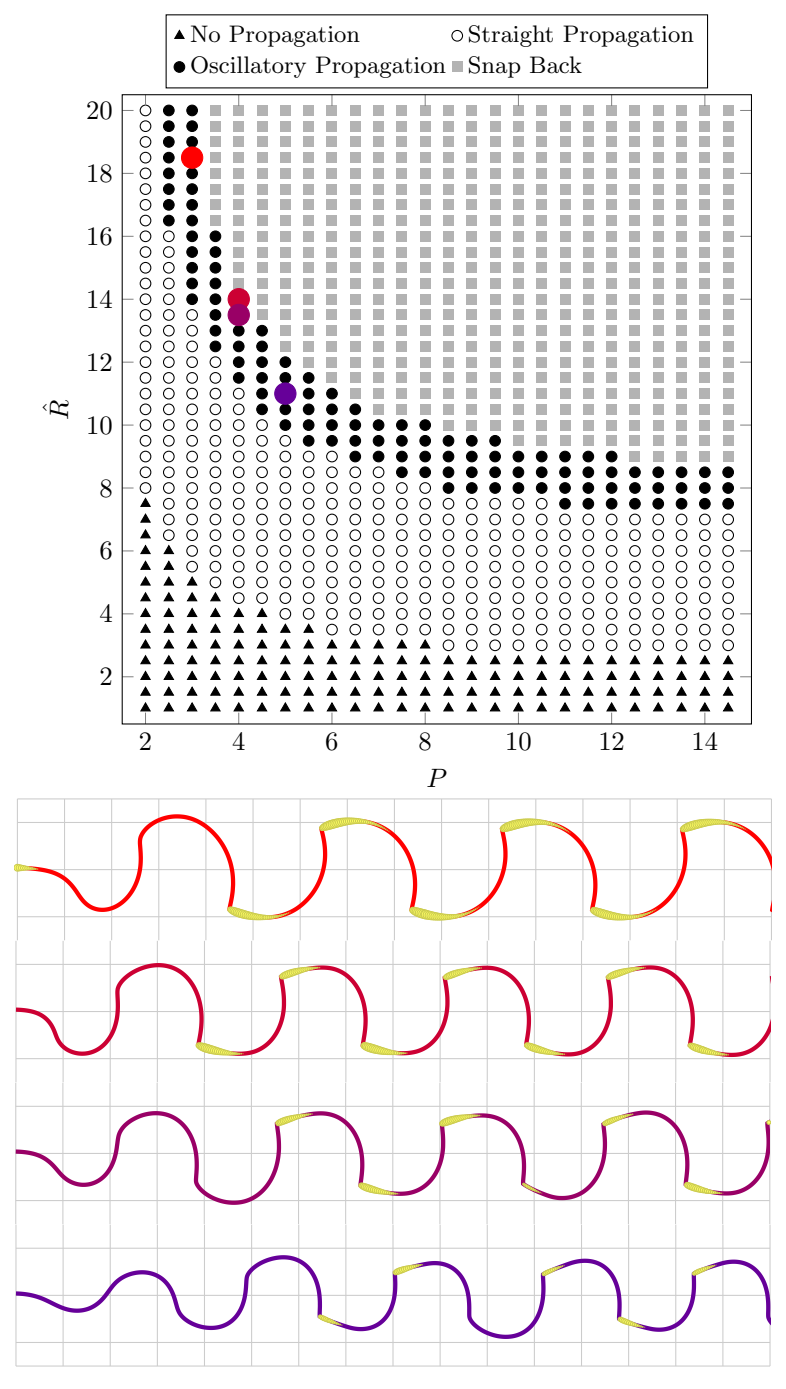


Figure 20: The crack propagates supercritically for short periods of time (namely  $K_I > K_C$ ). These periods are illustrated here by highlighting portions of the crack paths with yellow markers, where the size of the marker is correlated to the overstress  $(K_I - K_C)$ .

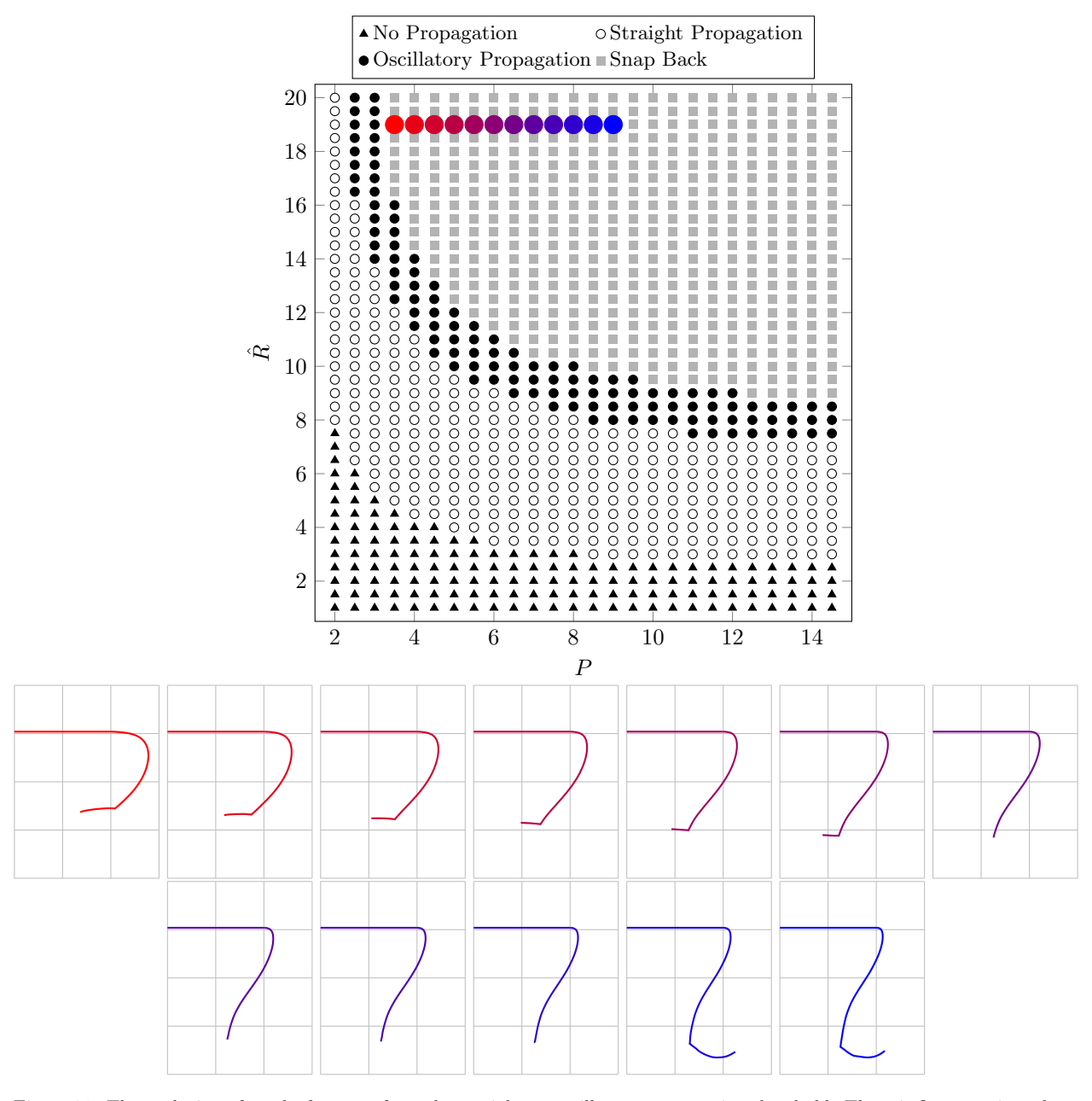


Figure 21: The evolution of cracks far away from the straight-to-oscillatory-propagation threshold. There is first a region where the crack turns back and arrest, and later, with enough energy (i.e. P sufficiently large), the crack is capable of continuing propagating.

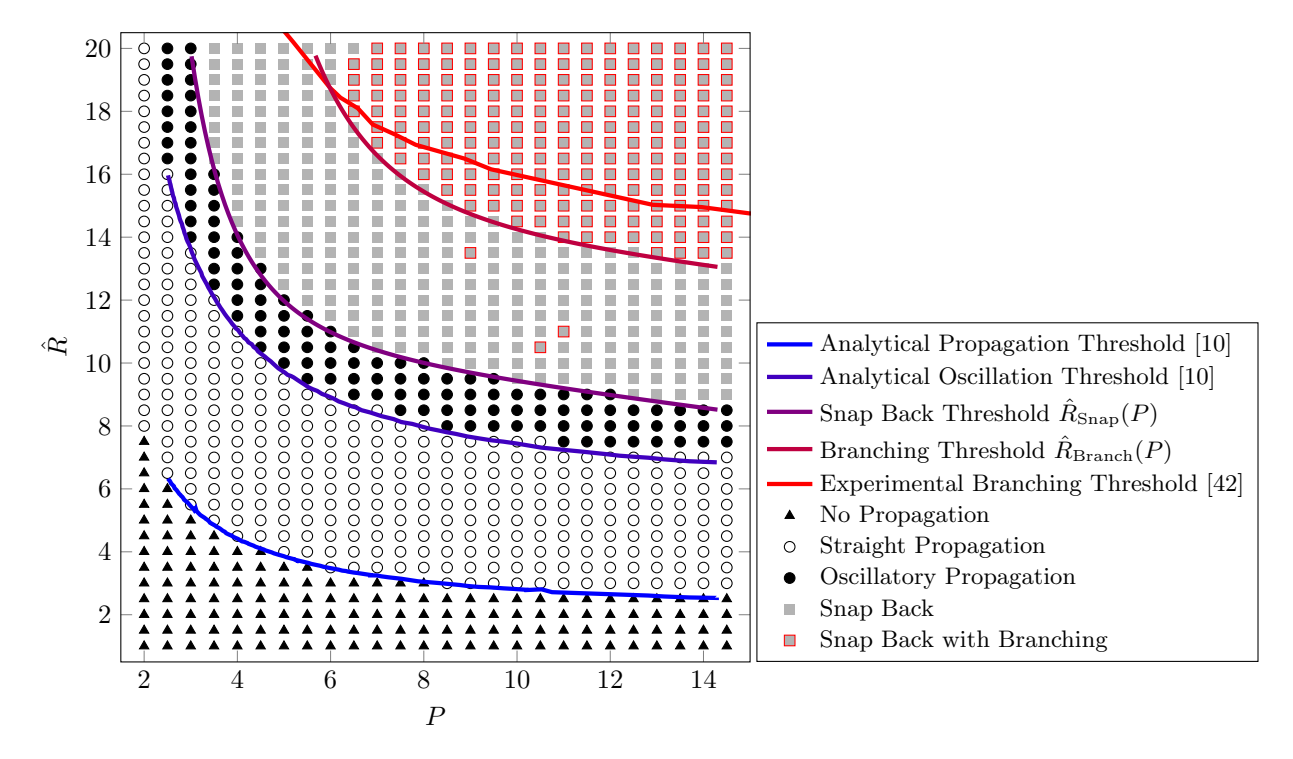


Figure 22: The squares with a red border indicate the points in phase space that satisfy the heuristic crack branching criterion stated by (13). Also shown are the newly identified thresholds for snap-back and branching,  $\hat{R}_{\mathrm{Snap}}(P)$  and  $\hat{R}_{\mathrm{Branch}}(P)$ , respectively, and a comparison of the heuristic branching threshold with the experimental results of [?]. Expressions for  $\hat{R}_{\operatorname{Snap}}(P)$  and  $\hat{R}_{\operatorname{Branch}}(P)$  are provided in Appendix B.

We conclude by highlighting that an intuitive explanation of the emergence and behaviors of the oscillations remains elusive. It would be also interesting to perform some time-resolved calculations of the dynamic fracture excursions the crack undergoes, to both better study the emergence of branching as well as to compare with the extension to the quasistatic evolution here. A priori, it would be expected for both to be similar for small departures of  $K_I/K_C$  from 1.

## Appendix A. Derivation of the Interaction Integral for Thermoelasticity

In this appendix we present a derivation of the Interaction Integral used in this work which accounts for the temperature field. The final result is given in (A.12). The notation presented herein follows that of [?]. In ? ], if u solves the linear elasticity problem

$$-\operatorname{div}(\mathbb{C}:\operatorname{grad}\boldsymbol{u})=\boldsymbol{b}, \quad \forall \boldsymbol{x}\in\Omega$$
(A.1)

$$(\mathbb{C}: \operatorname{grad} \boldsymbol{u})\boldsymbol{n} = \overline{\boldsymbol{t}}, \quad \forall \boldsymbol{x} \in \partial_{\tau}\Omega$$
(A.2)

then the Interaction Integral is given by

$$\hat{\mathcal{I}}\left[\operatorname{grad}\boldsymbol{u},\boldsymbol{\beta}^{\operatorname{aux}}\right] = \int_{B_{\rho}(\boldsymbol{x}_{\top})\cap\Gamma} \delta\boldsymbol{\gamma} \cdot \overline{\boldsymbol{\tau}}\left(\operatorname{grad}\boldsymbol{u},\boldsymbol{\beta}^{\operatorname{aux}}\right) dS \tag{A.3}$$

$$-\int_{B_{\rho}(\boldsymbol{x}_{\top})\backslash\Gamma} \overline{\boldsymbol{\Sigma}} \left(\operatorname{grad} \boldsymbol{u}, \boldsymbol{\beta}^{\operatorname{aux}}\right) : \operatorname{grad} \delta \boldsymbol{\gamma} \, dV \tag{A.4}$$

$$-\int_{B_{\rho}(\boldsymbol{x}_{\top})\backslash\Gamma} \overline{\boldsymbol{\Sigma}} \left(\operatorname{grad} \boldsymbol{u}, \boldsymbol{\beta}^{\operatorname{aux}}\right) : \operatorname{grad} \delta \boldsymbol{\gamma} \, dV$$

$$-\int_{B_{\rho}(\boldsymbol{x}_{\top})\backslash\Gamma} \delta \boldsymbol{\gamma} \cdot \overline{\Lambda} \left(\operatorname{grad} \boldsymbol{u}, \boldsymbol{\beta}^{\operatorname{aux}}\right) \, dV,$$
(A.4)

where  $B_{\rho}(\mathbf{x}_{\top})$  is a ball of radius  $\rho$  centered at the crack tip,

$$\overline{\tau} (\operatorname{grad} u, \beta^{\operatorname{aux}}) = \operatorname{grad} u : \mathbb{C} : \beta^{\operatorname{aux}} n - \operatorname{grad} u^{\top} \mathbb{C} : \beta^{\operatorname{aux}} n - \beta^{\operatorname{aux}} \overline{t},$$
 (A.6)

$$\overline{\Lambda} (\operatorname{grad} \boldsymbol{u}, \boldsymbol{\beta}^{\operatorname{aux}}) = \operatorname{grad} \boldsymbol{u} : \operatorname{grad} (\mathbb{C} : \boldsymbol{\beta}^{\operatorname{aux}}) - (\mathbb{C} : \operatorname{grad} \boldsymbol{u}) : (\operatorname{grad} \boldsymbol{\beta}^{\operatorname{aux}})^{\top} 
- \operatorname{grad} \boldsymbol{u}^{\top} \operatorname{div} (\mathbb{C} : \boldsymbol{\beta}^{\operatorname{aux}}) + \boldsymbol{\beta}^{\operatorname{aux}}^{\top} \boldsymbol{b}$$
(A.7)

and the interaction energy momentum tensor is defined as

$$\overline{\boldsymbol{\Sigma}}\left(\operatorname{grad}\boldsymbol{u},\boldsymbol{\beta}^{\operatorname{aux}}\right) = \operatorname{grad}\boldsymbol{u}: \mathbb{C}: \boldsymbol{\beta}^{\operatorname{aux}}\mathbf{1} - \operatorname{grad}\boldsymbol{u}^{\top}\boldsymbol{\sigma}\left(\boldsymbol{\beta}^{\operatorname{aux}}\right) - \boldsymbol{\beta}^{\operatorname{aux}}^{\top}\boldsymbol{\sigma}\left(\operatorname{grad}\boldsymbol{u}\right).$$

Expressions for the auxiliary gradient field  $\beta^{\text{aux}}$  and the material velocity  $\delta \gamma$  are provided in [?].

An important assumption in the previous form is that the material obeys reciprocity (i.e.  $\mathbb{C}$  has major symmetry). As written, the thermoelastic response in Problem 2.2 does not obey reciprocity; by separating out the thermal contributions, the balance of momentum equations can be rewritten such that

$$-\operatorname{div}\left(\mathbb{C}:\operatorname{grad}\boldsymbol{u}\right)=\boldsymbol{b}(\mathsf{T}),\quad\forall\boldsymbol{x}\in\Omega,\tag{A.8}$$

$$(\mathbb{C}: \operatorname{grad} \boldsymbol{u}) \, \boldsymbol{n} = \overline{\boldsymbol{t}}(\mathsf{T}), \quad \forall \boldsymbol{x} \in \partial_{\tau} \Omega, \tag{A.9}$$

where

$$\boldsymbol{b}(\mathsf{T}) = \zeta \operatorname{grad} \mathsf{T},\tag{A.10}$$

$$\bar{\boldsymbol{t}}(\mathsf{T}) = -\zeta \mathsf{T} \boldsymbol{n}. \tag{A.11}$$

Therefore the evaluation of the Interaction Integral for problems in thermoelasticity can be obtained by treating the thermoelastic problem as a linear elasticity problem where boundary tractions and body forces are non-zero and given by (A.11) and (A.10), respectively. With the above, one may readily obtain a value of  $\hat{\mathcal{I}}$  by replacing (A.11) and (A.10) in (A.6) and (A.7), respectively, and simply evaluating (A.5).

It is worthwhile noting that the temperature field is not smooth, with a discontinuity in the gradient at the cold front,  $x_C$ . Hence integrating numerically the gradient of the temperature (which arises from the term associated with b(T)) can yield poor accuracy. To alleviate this shortcoming, we simply manipulated the expression of  $\hat{\mathcal{I}}$  to obtain a formulation that does not require the evaluation of the derivative of the temperature field. Namely, the additional terms associated with the temperature field are given by

$$\begin{split} -\int_{B_{\rho}(\boldsymbol{x}_{\top})\cap\Gamma} \delta\boldsymbol{\gamma}\cdot\boldsymbol{\beta}^{\mathrm{aux}\;\top}\overline{\boldsymbol{t}}(\mathsf{T})dS - \int_{B_{\rho}(\boldsymbol{x}_{\top})\backslash\Gamma} \delta\boldsymbol{\gamma}\cdot\boldsymbol{\beta}^{\mathrm{aux}\;\top}\boldsymbol{b}\,dV \\ &= \int_{B_{\rho}(\boldsymbol{x}_{\top})\cap\Gamma} \mathsf{T}\zeta\delta\boldsymbol{\gamma}\cdot\boldsymbol{\beta}^{\mathrm{aux}\;\top}\boldsymbol{n}dS - \int_{B_{\rho}(\boldsymbol{x}_{\top})\backslash\Gamma} \mathrm{div}(\zeta\mathsf{T}\boldsymbol{\beta}^{\mathrm{aux}}\delta\boldsymbol{\gamma})dV \\ &+ \int_{B_{\rho}(\boldsymbol{x}_{\top})\backslash\Gamma} \zeta\mathsf{T}\left(\boldsymbol{\beta}^{\mathrm{aux}\;\top}: \mathrm{grad}\,\delta\boldsymbol{\gamma} + \delta\boldsymbol{\gamma}\cdot\mathrm{div}\,\boldsymbol{\beta}^{\mathrm{aux}\;\top}\right)\,dV \\ &= \int_{B_{\rho}(\boldsymbol{x}_{\top})\backslash\Gamma} \zeta\mathsf{T}\left(\boldsymbol{\beta}^{\mathrm{aux}\;\top}: \mathrm{grad}\,\delta\boldsymbol{\gamma} + \delta\boldsymbol{\gamma}\cdot\mathrm{div}\,\boldsymbol{\beta}^{\mathrm{aux}\;\top}\right)\,dV \end{split}$$

where we integrated by parts the second term of the first line, and used the divergence theorem to make the sum of the first two terms in the second line exactly zero. Therefore, the final form of the Interaction

Table B.2: Coefficients of the posynomial expression of equation (B.1).

	$\hat{R}_{\mathrm{Snap}}(P)$	$\hat{R}_{\mathrm{Branch}}(P)$
$\overline{a}$	321.362	3259.351
b	3.213	3.676
c	11.058	15.174
d	-0.182	-0.161

Integral is

$$\mathcal{I}\left[\operatorname{grad}\boldsymbol{u},\boldsymbol{\beta}^{\operatorname{aux}}\right] = \int_{B_{\rho}(\boldsymbol{x}_{\top})\cap\Gamma} \delta\boldsymbol{\gamma} \cdot \overline{\boldsymbol{\tau}}'(\operatorname{grad}\boldsymbol{u},\boldsymbol{\beta}^{\operatorname{aux}}) \, dS \\
- \int_{B_{\rho}(\boldsymbol{x}_{\top})\setminus\Gamma} \overline{\boldsymbol{\Sigma}}\left(\operatorname{grad}\boldsymbol{u},\boldsymbol{\beta}^{\operatorname{aux}}\right) : \operatorname{grad}\delta\boldsymbol{\gamma} \\
- \int_{B_{\rho}(\boldsymbol{x}_{\top})\setminus\Gamma} \overline{\boldsymbol{\Lambda}}'(\operatorname{grad}\boldsymbol{u},\boldsymbol{\beta}^{\operatorname{aux}}) \cdot \delta\boldsymbol{\gamma} \, dV, \\
+ \int_{B_{\rho}(\boldsymbol{x}_{\top})\setminus\Gamma} \zeta \mathsf{T}\left(\boldsymbol{\beta}^{\operatorname{aux}\top} : \operatorname{grad}\delta\boldsymbol{\gamma} + \delta\boldsymbol{\gamma} \cdot \operatorname{div}\boldsymbol{\beta}^{\operatorname{aux}\top}\right) \, dV$$
(A.12)

where

$$\overline{\tau}' (\operatorname{grad} \boldsymbol{u}, \boldsymbol{\beta}^{\operatorname{aux}}) = \overline{\tau} (\operatorname{grad} \boldsymbol{u}, \boldsymbol{\beta}^{\operatorname{aux}}) + \boldsymbol{\beta}^{\operatorname{aux}} \overline{t} \overline{t} (\mathsf{T}) 
= \operatorname{grad} \boldsymbol{u} : \mathbb{C} : \boldsymbol{\beta}^{\operatorname{aux}} \boldsymbol{n} - \operatorname{grad} \boldsymbol{u}^{\top} (\mathbb{C} : \boldsymbol{\beta}^{\operatorname{aux}}) \boldsymbol{n}, \qquad (A.13)$$

$$\overline{\Lambda}' (\operatorname{grad} \boldsymbol{u}, \boldsymbol{\beta}^{\operatorname{aux}}) = \overline{\Lambda} (\operatorname{grad} \boldsymbol{u}, \boldsymbol{\beta}^{\operatorname{aux}}) - \boldsymbol{\beta}^{\operatorname{aux}} \overline{t} \boldsymbol{b} (\mathsf{T}) 
= \operatorname{grad} \boldsymbol{u} : \operatorname{grad} (\mathbb{C} : \boldsymbol{\beta}^{\operatorname{aux}}) - (\mathbb{C} : \operatorname{grad} \boldsymbol{u}) : (\operatorname{grad} \boldsymbol{\beta}^{\operatorname{aux}})^{\top} 
- \operatorname{grad} \boldsymbol{u}^{\top} \operatorname{div} (\mathbb{C} : \boldsymbol{\beta}^{\operatorname{aux}}). \qquad (A.14)$$

### Appendix B. Coefficients of best fit polynomials for computed thresholds

We provide in what follows analytical expressions for the snap-back and branching thresholds. The expressions are a result of fitting a function

$$f(x) = \frac{a}{x^b} + c + dx \tag{B.1}$$

in the least square sense to the a set of data points sampled from Fig. 22. The coefficients for each threshold are given in Table B.2 to three decimal places and the functions are plotted in Fig. 22.

### Acknowledgements

The authors would like to thank Prof. Matteo Negri from University of Pavia, Italy, for his insight into the crack evolution described in this work. This work was supported by NSF-CMMI-166245, NSF-CMMI-1301396, and Army Research Grant W911NF-07-2-0027.